BETA AND GAMMA VIBRATIONAL BANDS IN DEFORMED NUCLEI

Thesis by

Larry Shelton Varnell

In Partial Fulfillment of the Requirements

For the Degree of

Doctor of Philosophy

California Institute of Technology

Pasadena, California

1969

(Submitted May 19, 1969)

ACKNOWLEDGMENTS

I would like to thank Professor Felix Boehm for his advice and encouragement during the completion of this thesis.

I am also grateful to Dr. Christian Gunther for valuable suggestions on the direction of this research, and to Dr. Edwin Seltzer for many discussions on the results of the experiments.

Dr. John Trischuk and Dr. David Bowman participated in some of the experiments, and their assistance is greatly appreciated. Dr. Elton Kaufmann offered useful advice on the least squares program. Herb Henrickson and Bob Marcley were especially helpful with equipment used in the experiments.

I would also like to acknowledge the encouragement and insight provided by Dr. Lew Cocke.

Financial assistance was provided by the California Institute of Technology. The research was supported by the Atomic Energy Commission.

Abstract

Energies and relative intensities of gamma transitions in ^{152}Sm, ^{152}Gd, ^{154}Gd, ^{166}Er, and ^{232}U following radioactive decay have been measured with a Ge(Li) spectrometer. A peak fitting program has been developed to determine gamma ray energies and relative intensities with precision sufficient to give a meaningful test of nuclear models. Several previously unobserved gamma rays were placed in the nuclear level schemes. Particular attention has been paid to transitions from the beta and gamma vibrational bands, since the gamma ray branching ratios are sensitive tests of configuration mixing in the nuclear levels. As the reduced branching ratios depend on the multipolarity of the gamma transitions, experiments were performed to measure multipole mixing ratios for transitions from the gamma vibrational band. In ^{154}Gd, angular correlation experiments showed that transitions from the gamma band to the ground state band were predominantly electric quadrupole, in agreement with the rotational model. In ^{232}U, the internal conversion spectrum has been studied with a Si(Li) spectrometer constructed for electron spectroscopy. The strength of electric monopole transitions and the multipolarity of some gamma transitions have been determined

from the measured relative electron intensities.

The results of the experiments have been compared with the rotational model and several microscopic models. Relative B(E2) strengths for transitions from the gamma band in ^{232}U and ^{166}Er are in good agreement with a single parameter band mixing model, with values of $z_2 = 0.025(10)$ and $0.046(2)$, respectively. Neither the beta nor the gamma band transition strengths in ^{152}Sm and ^{154}Gd can be accounted for by a single parameter theory, nor can agreement be found by considering the large mixing found between the beta and gamma bands. The relative B(E2) strength for transitions from the gamma band to the beta band in ^{232}U is found to be five times greater than the strength to the ground state band, indicating collective transitions with strength approximately 15 single particle units.

TABLE OF CONTENTS

I. INTRODUCTION

The study of gamma rays following nuclear beta decay and electron capture has provided a large part of the available data on decay schemes and nuclear energy levels. From these results, nuclear models have been proposed which correlate properties of different nuclei and give excitation energies, spins, magnetic dipole and electric quadrupole moments, decay modes, and lifetimes.

If one examines the level structure of nuclei in the rare earth region, there is a remarkable contrast between odd-A and even-even isotopes. Numerous excited states appear in odd-A isotopes with a spacing of 50-100 keV, while in even-even isotopes, there are only one or two excited states at low energy. There is a "gap" of energy levels below about 1 MeV. Above this energy, the states are more numerous and closely spaced. This energy gap, as well as the long established strongly deformed shape of all nuclei in the rare earth region provide evidence for two important residual interactions: the pairing force and the quadrupole force. Models using these interactions have been successfully used for microscopic calculations. On a macroscopic scale, the unified collective model has had exceptional success in

explaining the low-lying levels of deformed odd-A nuclei as 1) single particle excitations, 2) rotational excitations based on the single particle states, and 3) vibrational excitations.

In even-even nuclei, the few low-lying states are described as rotational excitations of the ground state. The excited states at about 1 MeV are: 1) two particle excitations, 2) rotational excitations based on these two particle excitations, and 3) nuclear shape vibrations.

All these classifications are greatly simplified descriptions of the complicated nuclear motion. In fact, we know that it is necessary to consider perturbations which lead to mixing between excited states as classified above. It turns out that both the energy of a level and the transition rate depend on the amount of mixing in a first order calculation. In this sense the branching ratios of transitions to different levels in a rotational band are sensitive tests of the model since they are strongly affected by admixtures of other levels.

Above the ground state band, the most prominent feature of deformed nuclei is the existence of beta and gamma vibrational bands. Measurements of the branching ratios from the gamma band in strongly deformed nuclei showed good agreement with predictions of the rotational model if the first order

band mixing corrections were included. [1] Similar experiments[2, 3] for nuclei in the transition region from spherical to deformed intrinsic shape near Sm showed good agreement with this model for the gamma band but not for the beta band. The failure of the band mixing model would imply a breakdown in the fundamental rotational relationship, since the band mixing treatment used does not depend on the intrinsic structure of the bands. [4]

In this thesis a study of branching ratios in ^{152}Sm and ^{154}Gd, ^{166}Er, and ^{232}U was undertaken with a Ge(Li) spectrometer. It is found that for ^{166}Er the observations are well explained with a one parameter band mixing model. For ^{152}Sm and ^{154}Gd, no agreement with a single parameter band mixing model can be found for either the beta band or the gamma band.

In ^{232}U previous experiments [5] had given evidence for strongly collective transitions from the gamma band to the beta band, although these transitions are forbidden in the simple vibrational model. A large degree of mixing of the two vibrational bands was necessary to explain the observed branching ratios; however, these experiments were not performed with sufficient accuracy to test the validity of the model.

The rotational model also gives rules for the multipolarity of transitions between bands. [6] For transitions from the gamma

band(K=2) to the ground state band(K=0), the difference in the K quantum number is Δ K=2, so the transitions should be E2. Because of band mixing, however, M1 admixtures are possible. In deriving electric quadrupole branching ratios from the experimental relative intensities, it is necessary to know the amount of M1 admixture in the gamma ray transitions. These mixing ratios can be obtained from angular correlation experiments. Experiments of this sort have been reported in the literature for transitions from the gamma band to the ground state band in ^{154}Gd;[7, 8] however, they do not agree with each other. Measurements of transitions from the beta band to the ground state band are more difficult, and evidence for M1 admixtures is inconclusive.[9, 10] We have performed angular correlation experiments in ^{154}Gd to measure the multipolarity of transitions from the gamma band to the ground state band. These results are discussed in this thesis.

Multipolarities of transitions can also be determined from the intensities of internal conversion electrons emitted in the decay. Calculated conversion coefficients[11] are accurate to a few per cent and can be used to determine multipole admixtures. A solid state electron spectrometer was used to study the electron spectrum of ^{232}Pa.

To achieve the accuracy necessary for a critical comparison of experimental intensities with nuclear model predictions, a computer program was developed. It serves to determine the relative intensity of lines recorded by the Ge(Li) spectrometer.

Finally, a discussion of recent microscopic calculations is given at the end of the thesis.

II. THE ROTATIONAL MODEL

A. Introduction

The unified collective model[12] combines features of the independent particle shell model[13] and the collective hydrodynamic model.[14] Nearly independent nucleons move in a deformed potential which is slowly varying because of the rotation of the nuclear shape. Because the rotation of the shape is slow compared to the frequency of the particle orbits (as evidenced by the small spacing of the rotational levels compared to the intrinsic excitations), the adiabatic approximation introduced by A. Bohr is useful.[15] In this approximation the nuclear Hamiltonian can be divided into collective (rotational) and intrinsic parts, and the nuclear wave function is a product of the respective eigenfunctions of the collective and intrinsic Hamiltonian. The interaction between the intrinsic and rotational motions is assumed to be small enough to be treated by perturbation methods. The demonstration of the validity of the adiabatic assumption from the viewpoint of the nuclear many body problem is quite difficult, but the results following from the assumption are quite simple and agree well with experiment.

B. Wave Functions, Energy Levels, and Reduced Branching Ratios

The nuclear Hamiltonian can be written in the form[16]

$$H = H_{intr} + T_{rot} + H_{coupl}$$

where H_{intr} = particle Hamiltonian

T_{rot} = kinetic energy of rotation

H_{coupl} = coupling of the intrinsic and rotational motion.

The wave function is a product:

$$\Psi \sim D^{I}_{MK}(\vartheta)\ X(x')$$

where ϑ represents the orientation of the intrinsic coordinate system x'. The quantum numbers I, M, and K are represented in Figure 1. The $D^{I}_{MK}(\vartheta)$ are eigenfunctions of T_{rot} (with the exception of two terms) and the $X(x')$ are the wave functions of the intrinsic motion. Using these wave functions, the energy levels of the ground state rotational band are

$$E_I = \frac{\hbar^2}{2\mathcal{I}}\ I(I+1)$$

(See Appendix A.)

Reduced branching ratios for E2 transitions from a level of spin I_iK_i to levels I_fK_f and $I_f'K_f$ in a rotational band K_f are given by

$$\frac{B(E2)}{B'(E2)} = \frac{\langle I_i 2K_i (K_i - K_f) \mid I_f K_f\rangle^2}{\langle I_i 2K_i (K_i - K_f) \mid I_f' K_f\rangle^2}$$

These ratios can be readily measured, since for a pure transition

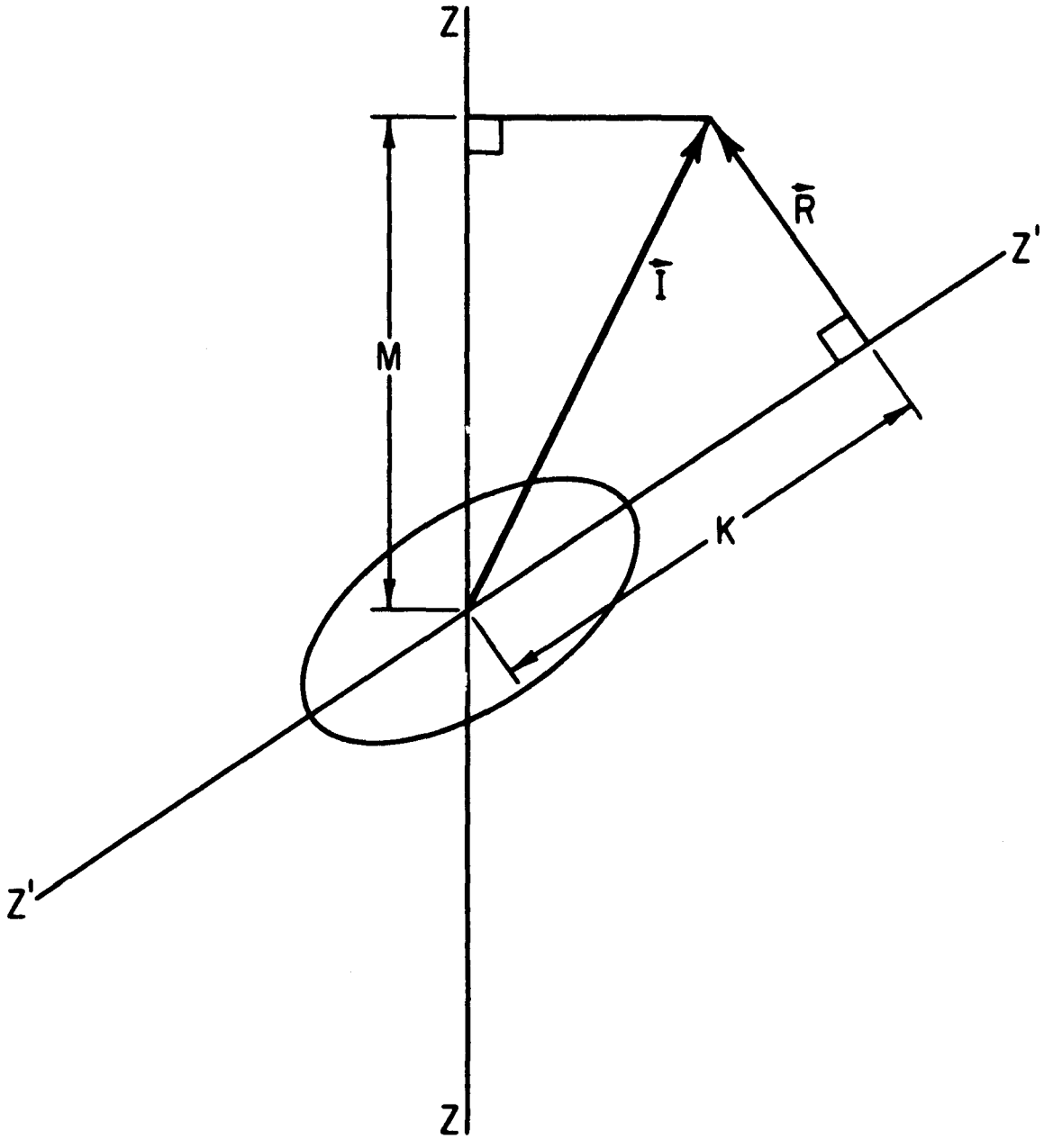

Figure 1

Coupling scheme for deformed nuclei. I is the total angular momentum of the nucleus. K and M are the projections of I on the symmetry axis Z' and the space fixed axis Z, respectively. R is the collective angular momentum.

$B((M(\lambda)) \sim {}^{I}\gamma / E_{\gamma}^{2\lambda+1}$ where I_{γ} is the measured relative intensity and E_{γ} is the energy of the gamma ray of multipolarity λ.

A discussion of vibrational states is also given in Appendix A.

C. Rotational-Particle Coupling

The $D^{I}_{MK}\chi_{K}$ functions are not eigenfunctions of the operator $\vec{I}\cdot\vec{J}$. This term, called the Coriolis interaction, mixes states with K values differing by unity. Mixing of the K=0 ground state band and the K=0 beta and K=2 gamma band can occur by Coriolis interaction in second order through K=1 bands. Alternatively, the interaction can be expanded in powers of the angular momentum operators I and J (J is denoted by h in this representation). A review of this expansion is given by Marshalek.[17]

$$H_{coupl} = \sum_{i=1} H^{(i+1)}$$

$$H^{(i+1)} = h_{+i} I^{i}_{-} + h_{-i} I^{i}_{+}$$

$$I_{\pm} D^{I}_{MK} = [\,(I\mp K)(I\pm K+1)\,]^{1/2} D^{I}_{M\ K\pm 1}$$

$$\langle X_{-K} \mid h_{-K} \mid X_{o}\rangle = (-)^{K} \langle X_{+K} \mid h_{+} \mid X_{o}\rangle$$

The terms which mix the ground state with the gamma and beta bands are $h_0(I_1^2 + I_2^2) + h_2 I_-^2 + h_{-2} I_+^2$.

Using first order perturbation theory, the ground-state wave function is $|00I\rangle' = |00I\rangle - \epsilon_0 I(I+1)\ |10I\rangle - \epsilon_2[2I(I+1) \times (I-1)(I+2)]^{1/2}\ |12I\rangle$

while the perturbed beta-and gamma-band functions, respectively, are given by

$$|10I\rangle' = |10I\rangle + \epsilon_0 I(I+1)\ |00I\rangle$$

$$|12I\rangle' = |12I\rangle + \epsilon_2 \tfrac{1}{2}\,(1+(-1)^{I})[2I(I+1)(I-2)(I+2)]^{1/2}\,|00I\rangle\,,$$

where the reduced mixing amplitudes are

$$\epsilon_0 = \frac{\langle 10|h_0|00\rangle}{E_{10} - E_{00}} \quad , \qquad \epsilon_2 = \frac{\langle 12|h_2|00\rangle}{E_{12} - E_{00}} \quad .$$

The first order correction to the gamma-ray branching is expressed in terms of a mixing parameter z. In nuclei with both beta and gamma bands, there is a parameter, z_0 and z_2, for each band respectively. The relative B(E2) ratios are given by

$$B(E2,\ I_i \rightarrow I_f)_{exp} = B(E2,\ I_iK = 0 \rightarrow I_fK = 0)[1 + z_0(I_f(I_f+1) - I_i(I_i+1))]^2$$

with

$$z_0 = -\epsilon_0 \frac{\langle 00|Q(E2,0)|00\rangle}{\langle 10|Q(E2,0)|00\rangle}$$

for the beta band, and

$$B(E2, I_i \rightarrow I_f)_{exp} = B(E2, I_iK = 2 \rightarrow I_fK = 0)[1 + z_2 f_2(I_iI_f)]^2$$

$$z_2 = -\sqrt{24}\,\epsilon_2 \frac{\langle 00|Q(E2,0)|00\rangle}{\langle 12|Q(E2,0)|00\rangle}$$

for the gamma band. The value of the correction is given in column 3, Table 1, for various spin values.

Michailov[18] has given a form of the band mixing correction which is valid for all multipoles. For electric quadrupole transitions, the result is

$$B(E2, I_iK=2 \rightarrow I_fK=0) = 2\langle I_i 2\ 2\ -2|\ I_f\ 0\rangle^2 \left\{ M_1 + M_2 [I_f(I_f+1) - I_i(I_i+1)] \right\}^2$$

The relation to the z_2 parameter is given by

$$z_2 = \frac{2\,M_2}{M_1 - 4M_2}$$

The outstanding agreement of the model for a large number of levels in the gamma band of ^{166}Er is shown in Figure 2, taken from Mottelson's paper.[4] Other examples of the success of the first order band mixing model are given there.

If the two vibrational bands mix with each other, the branching of the gamma band and the beta band to the ground state would be altered, as discussed by Lipas.[19] While the ground state wave function is unchanged, the beta- and gamma-band wave functions are, respectively,

$$|10I\rangle' = |10I\rangle + \epsilon_0 I(I+1)\,|00I\rangle - \epsilon_{\beta\gamma}[2I(I-1)(I+1)(I+2)]^{1/2}\,|12I\rangle$$

$$|12I\rangle' = |12I\rangle + \epsilon_2 \tfrac{1}{2}[1 + (-1)^I][2I(I+1)(I-1)(I+2)]^{1/2}\,|00I\rangle + \epsilon_{\beta\gamma}\tfrac{1}{2}[1 + (-1)^I][2I(I-1)(I+1)(I+2)]^{1/2}\,|10I\rangle$$

$$\epsilon_{\beta\gamma} = \frac{\langle 12|h_2|10\rangle}{E_{12} - E_{10}}.$$

The expressions for the reduced branching ratios are given in column 1.

So far we have assumed that the quadrupole moments of the gamma- and beta-band are equal to that of the ground state band. If this is not the case, and we consider only mixing of the

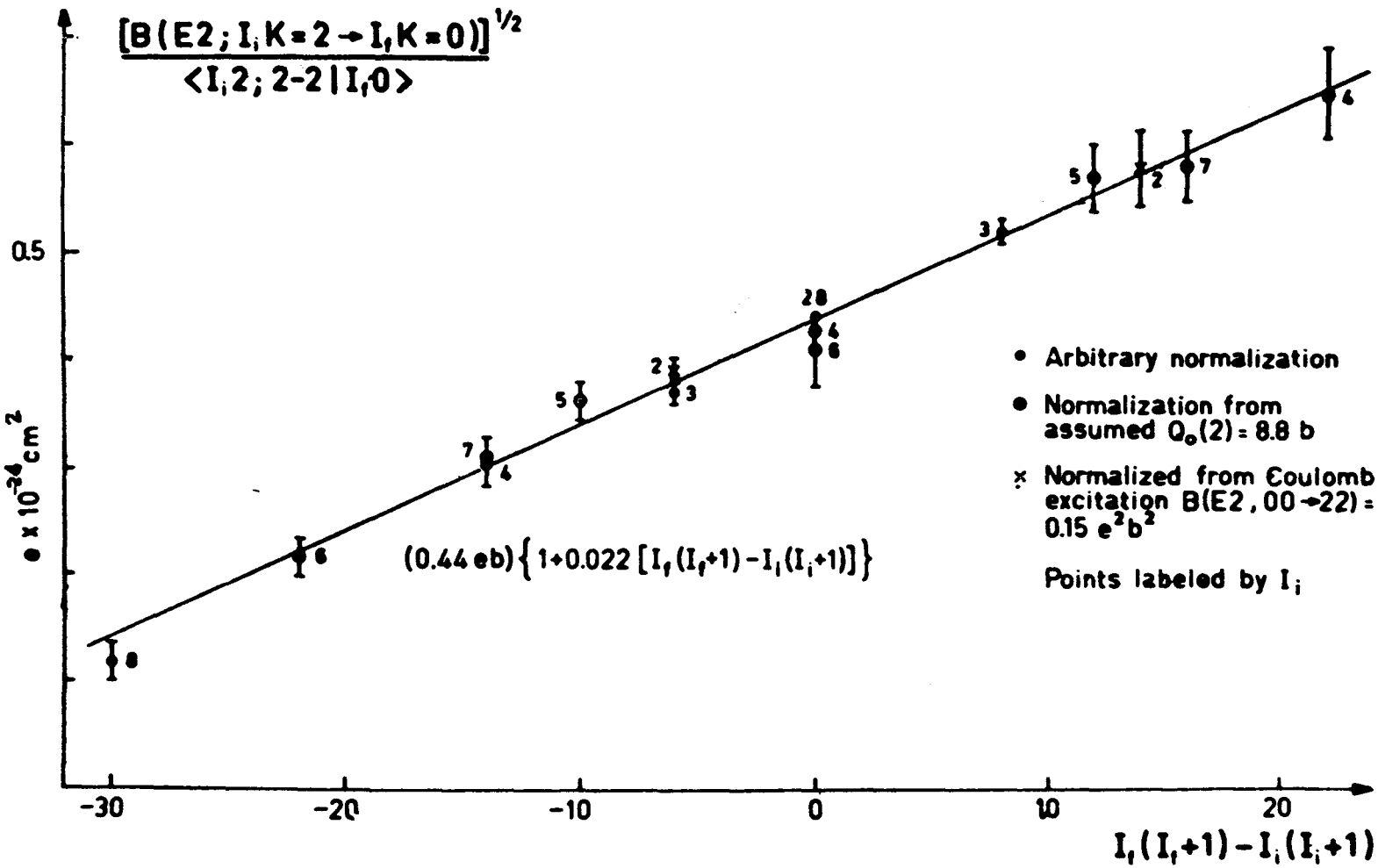

Figure 2

Relation of theoretical and observed B(E2) in ^{166}Er. Taken from reference 4.

gamma band and beta band with the ground-state band, and not with each other, the B(E2) ratios for the beta and gamma band, respectively, are given by

$$B(E2, I_i \longrightarrow I_f) = B(E2, I_i K = 0 \longrightarrow I_f K = 0) \times$$

$$\times \left[1 + a\, I_f\, (I_f + 1) - b\, I_i\, (I_i + 1) \right]^2$$

$$B(E2, I_i \longrightarrow I_f) = 2 \left\langle I_i 2\ 2\ -2 \middle| I_f\ 0 \right\rangle^2 \times$$

$$\times \left\{ M_1 + M_2 \left[I_f\, (I_f + 1) - I_i\, (I_i + 1) \right] \right.$$

$$\left. + M_3 \left[(I_f (I_f + 1) - I_i (I_i + 1))^2 - 2 (I_f\, (I_f + 1) + I_i (I_i + 1)) \right] \right\}^2$$

The B(E2) ratios are given in Table 1.

Table 1

Transition $\gamma \rightarrow$ G. S.		Rotational Value	$1-z_2 f_2$	Mixing of γ and β Bands	$Q_{22} \neq Q_{00}$
2	0	.70	$1-z_2$	$1-z_2+2z_3$	$1-6a+24b$
2	2	1.	$1+2z_2$	$1+2z_2-2z_3$	$1-24b$
2	4	.05	$1+9z_2$	$1+9z_2+12z_3$	$1+14a+144b$
3	2	2.5	$1-z_2$	$1-z_2$	$1-6a$
3	4	1.	$1+6z_2$	$1+6z_2$	$1+8a$
4	2	.34	$1-5z_2$	$1-5z_2+12z_3$	$1-14a+144b$
4	4	1.	$1+2z_2$	$1+2z_2-20/3z_3$	$1-80b$
4	6	.086	$1+13z_2$	$1+13z_2+30z_3$	$1+22a+360b$
5	4	1.75	$1-3z_2$	$1-3z_2$	
5	6	1.	$1+8z_2$	$1+8z_2$	

Transition $\beta \rightarrow$ G. S.		Rotational Value	$1-z_o f_o$	Mixing of γ and β Bands	$Q''_{00} \neq Q_{00}$
2	0	.70	$1-6z_o$	$1-6z_o-12z_4$	$1-6d$
2	2	1.	1	$1+12z_4$	$1+6c-6d$
2	4	1.8	$1+14z_o$	$1+14z_o-2z_4$	$1+20c-6d$
4	2	2.1	$1-14z_o$	$1-14z_o-30z_4$	$1+6c-20d$
4	4	1.	1	$1+54z_4$	$1+20c-20d$
4	6	1.75	$1+22z_o$	$1+22z_o-12z_4$	$1+42c-20d$

III. EXPERIMENTAL TECHNIQUES

A. Detectors

1. Lithium Drifted Germanium

The gamma ray studies described here have been made with a Ge(Li) detector. The principal feature of this detector is high energy resolution. The good linearity with incident energy allows energies to be measured in comparison with calibration standards. We include here a short discussion of our experimental equipment with regard to these characteristics.

The best resolution reported for Ge(Li) detectors is in the range of 300 ev FWHM for lines of 10-20 kev.[20] The line width is a fold of several components; noise associated with the preamplifier and following electronics, detector leakage current and charge collection effects, and statistical fluctuation in the amount of charge produced and collected per unit energy absorbed. At low energies, most of the width is due to the first component. At energies above 500 keV, the third effect predominates. The bias voltage on the detector should be high enough to collect the charge produced by the radiation, but not so high as to create large reverse currents across the diode. Good detectors can operate at over 200 volts per millimeter of depletion depth. The

resolution of the system used in the experiments described here was 2.8 keV FWHM for the 1.332 MeV line of ^{60}Co, with a bias of 2300 volts.

The full energy peak efficiency of the Ge(Li) detector for lines of 100 keV is about 80%, losses being in Compton events in the detector and absorption of the gamma rays in the inactive layer of the crystal.[21] For the detector used here, 5 cm^2 x 10 mm deep, the full energy peak efficiency for an energy of 1.5 MeV is about 1% of the efficiency at 100 keV. For a 7.6x7.6 cm NaI detector, the relative photopeak efficiency at 1.5 MeV is 17%.[22] At 5 cm distance between the source and detector, the NaI detector has a solid angle of 10%, our Ge(Li) 1%. Thus at the same distance from the source, the Ge(Li) detector has less than 1% of the absolute efficiency of the NaI for high energy lines. These considerations are most important in coincidence experiments. The method used for determining accurately the relative efficiency of the Ge(Li) detector is discussed in Section B.

The linearity of the Ge(Li) detector as a function of the incident energy is found to be better than the associated electronics (pre-amp, amplifier, multi-channel analyzer).[23] Energies can be determined to within 0.050 keV when sufficient calibration sources are available.

The rise time of pulses from a Ge(Li) detector is of the order of 10 - 100 nanoseconds,[24] depending on the geometry, purity of the crystal, and bias voltage. By using leading edge timing, time resolution of 20 ns FWHM is possible, and we have obtained resolution of better than 10 ns for lines with energy greater than 500 keV.

2. Lithium Drifted Silicon

The very low efficiency of Si(Li) detectors for gamma rays limits their use to x-ray and electron spectroscopy. In the experiments described here, the detectors were used solely for conversion electrons. A rough efficiency calibration (5-10%) was made with known intensities of conversion electrons from ^{154}Eu (16 y), and it was found that the 3 mm depletion depth of the detector gave complete absorption for electrons of energy up to 1.5 MeV. The efficiency was then taken to be 100% for electrons up to that energy.

B. Analysis of Gamma Ray Spectra

1. Introduction

This section describes a method for obtaining the energies and intensities of gamma ray transitions measured with a Ge(Li) detector. In developing the program for computer analysis, the following criteria were maintained: for a valid test of nuclear models, the relative intensities of gamma-transitions should be

measured to better than 5% and the energy to better than 0.1 keV.

Extensive programs for the analysis of NaI spectra have been reported in the literature.[25] In general, the response of the NaI spectrometer is measured as a function of energy using mono-energetic sources. A response function is determined for the system for each energy, using the photopeak, Compton distribution, and escape peaks. These response functions are then used to "strip" a more complicated spectrum with many gamma lines present. This procedure is necessary because photopeaks are often not separated by the relatively poor resolution of NaI detectors. In contrast to this, with the improved resolution of Ge(Li) detectors, photopeaks are often widely separated and located on a relatively flat background. Accurate intensity measurements should be possible using only the full energy peak.

In analyzing Ge(Li) spectra, several authors have used Gaussian shapes to fit the full energy peak or a portion of it.[1, 26, 27] However, as better resolution became available, through improvement of techniques in production of the detectors, but principally in the development of better field effect transistors (FET) in the preamplifier input stage, it became clear that the Gaussian did not give a satisfactory fit to the peak shape. The effects of amplifier pile-up, detector charge collection, and system drifts became

evident. There were several alternatives. First, an experimentally measured response function could be used, as with NaI detectors. Second, a Gaussian plus an orthogonal series could be fitted to the peak shape. The method described here is a third alternative; it consists of using an analytic function with parameters chosen to represent the response of the spectrometer system.

2. The Peak Fitting Program

The basic function used to fit the full energy peak is the fold of a Gaussian with an exponential (the complementary error function). At low energies, the width of the Gaussian is determined by the electronic noise of the system. As the energy of the gamma-ray increases, the width becomes larger from statistical processes connected with energy absorption in the detector. A quadratic background is used, primarily to help in fitting peaks near the Compton edges of higher energy lines.

Pile-up effects in the amplifier are simulated by folding high and low energy exponentials with the Gaussian (see Figure 3). The long tail observed on the low energy side is attributed to incomplete charge collection of hole-electron pairs due to recombination and trapping. This tail is simulated by a second complementary error function with the same center as the main

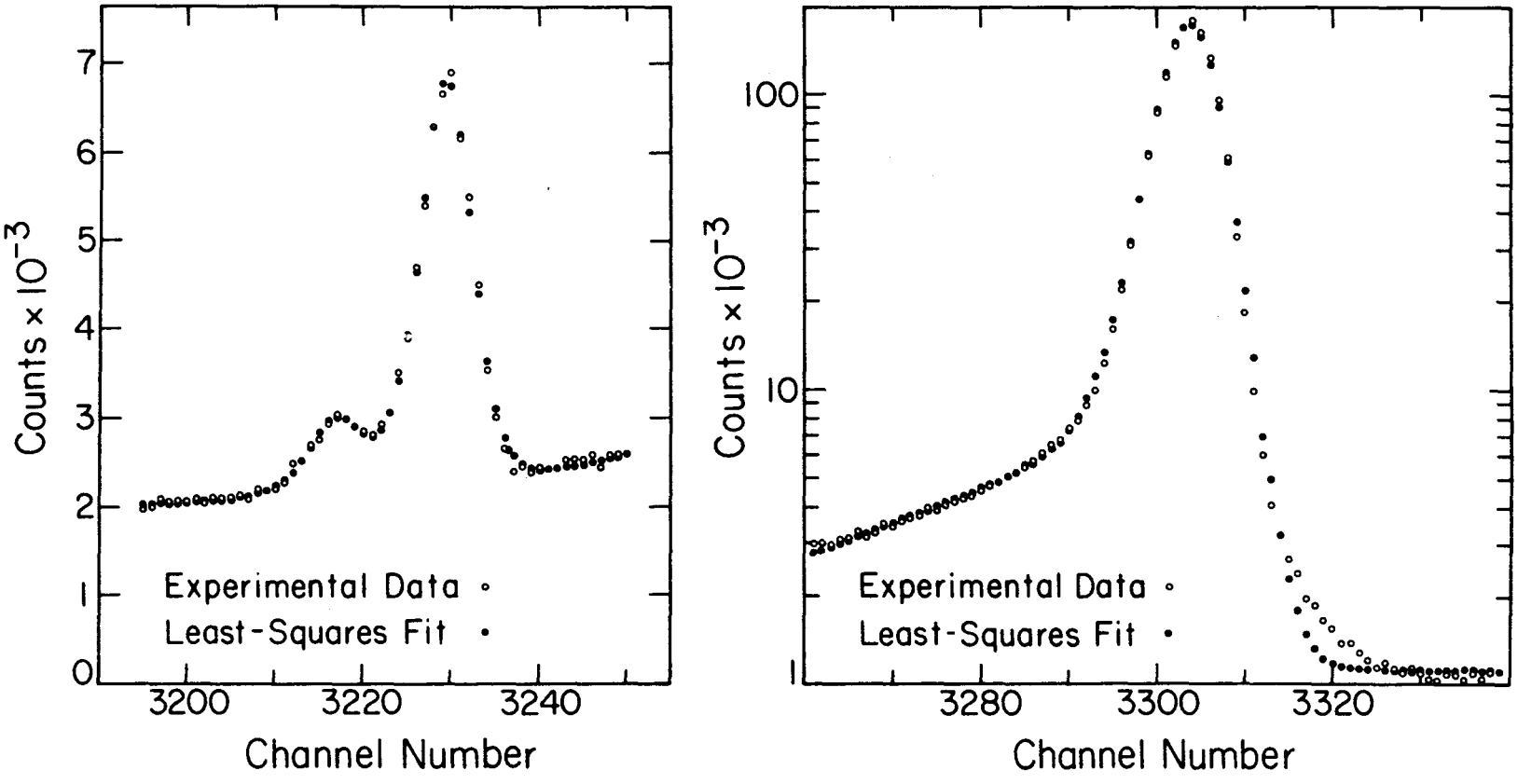

Figure 3

Examples of the peak fitting program. On the left, the 1241.6 and 1246.6 keV lines in ^{154}Gd; on the right, the 1274.4 keV line.

peak. The function adopted for a single full energy peak is as follows:

$$F = A\left\{ \frac{1}{2(\lambda_1+\lambda_2)} e^{(x-x_0)/\lambda_1 + \sigma^2/2\lambda_1^2} \left[1 - \mathrm{ERF}\left(\frac{x-x_0}{\sqrt{2}\sigma} + \frac{\sigma}{\lambda_1\sqrt{2}}\right)\right] \right.$$

$$+ \frac{1}{2(\lambda_1+\lambda_2)} e^{-(x-x_0)/\lambda_2 + \sigma^2/2\lambda_2^2} \left[1 - \mathrm{ERF}\left(\frac{-(x-x_0)}{\sqrt{2}\sigma} + \frac{\sigma}{\lambda_2\sqrt{2}}\right)\right]$$

$$\left. + \frac{B}{2\lambda_3} e^{(x-x_0)/\lambda_3 + \sigma^2/2\lambda_3^2} \left[1 - \mathrm{ERF}\left(\frac{x-x_0}{\sqrt{2}\sigma} + \frac{\sigma}{\lambda_3\sqrt{2}}\right)\right] \right\}$$

$$+ a + b(x-x_0) + c(x-x_0)^2$$

There are ten parameters in the function F:

position x_0

standard deviation σ

decay length, low energy λ_1

decay length, high energy λ_2

decay length, charge collection λ_3

two area parameters, A, B

three background parameters a, b, c.

The first two terms are the result of folding a Gaussian of width σ and center x_0 with exponentials of decay

length λ_1 and λ_2, centered at x_0. These terms represent the main peak, modified by pile-up of the singly-integrated and differentiated pulses. The third term is the long low energy tail attributed to incomplete charge collection. The remaining terms are the quadratic background.

Originally, all ten parameters were allowed to vary for each peak. It was found, however, that the parameters did not vary in a smooth manner with energy, within the assigned errors. So it was decided to measure the five parameters which determine the peak shape (λ_1, λ_2, λ_3, σ, B) as a function of energy, using single line sources of different energies. These five parameters were determined for each energy, then each parameter was fitted to a polynomial as a function of energy. In fitting a line, the value of these five parameters was determined from the polynomial fit and fixed. Only the peak position, area, and the three background parameters are allowed to vary in the fit. For more than one peak in the region fitted, only two instead of five additional parameters are added for each peak, the area and position; the same three background parameters are used for the entire region. Thus for two peaks there would be the five fixed parameters, and seven varying parameters; for three peaks nine varying parameters, etc. To insure consistency

in various runs, the energy scale on the analyzer was kept constant. This was accomplished by using a pulser fed through the preamplifier as a reference peak for the analyzer gain stabilizer. Fixing the parameters which determine the peak shape and fitting both the unknown and calibration lines in the same way also minimizes any small error in the peak shape.

3. The Nonlinear Fitting Program

The nonlinear least-squares fitting program used was developed by Marquardt [28] and programmed by Davidon [29] (IBM SHARE 3094). The objective is to minimize

$$\Phi = \sum_{i=1}^{n} \left[\frac{Y_i - F_i(p_j)}{\Delta Y_i} \right]^2$$

: where Y_i and ΔY_i are the measured value and error, respectively, at the ith data point X_i, and $F_i(p_j)$ is the value predicted by the function used in the fit. Initial estimates of the parameters are supplied as input data. The program then determines the direction and magnitude of the correction vector to the parameters. The method performs an optimum interpolation between the Taylor series method and the gradient method. When there are large correlations between parameters, the Taylor series method may not converge. The gradient method converges quite slowly after the first few iterations. After new values of the parameters are

obtained, Φ is calculated, and the iteration is repeated until the convergence criteria are met. The program must be supplied with convergency limits, data to be fitted, the function to be used and its derivatives, and the initial value of the parameters.

4. Spectrum Analysis

The program described above has been used in our laboratory for intensity and energy measurements[30, 31, 32] for several isotopes. Specific details of the measurements can be discussed in terms of the particular system used in these measurements. As the shape of the peak depended somewhat on the electronics used, all measurements were made using the same components. Effects due to pile-up and drifts were minimized by use of low counting rates, an amplifier with pole-zero cancellation, and gain stabilization on the multi-channel analyzer which corrected for drifts in the entire system. The Ge(Li) detector used was a 5 cm^2 x 10 mm planar detector manufactured by Ortec. The bias voltage was kept constant at 2300 volts supplied by batteries. It was found that the peak shape did not change on increasing the voltage from 1900 volts to 2500 volts. An Ortec 118A preamplifier with room temperature input was mounted on the cryostat. The amplifier was a Canberra 1416, with time constants 2 microsec., single differentiation and integration, pole-zero cancelled. The

analyzer was a Nuclear Data 161F, 4096 channel, with a ND gain stabilizer set on a peak supplied by a Tennelec TC800 pulser fed through the preamp. The stabilizer had a marked effect on the shape of the peaks, especially narrowing the region near the base. The lines of primary interest in the nuclei studied were below 1500 keV, so the energy scale of the analyzer was fixed with the maximum energy at approximately 1550 keV. The pulser was adjusted to approximately 1525 keV and the gain stabilizer set on the peak. Each calibration source was recorded separately at 20% dead time at ten cm distance from the face of the detector. No effect on the peak shape or efficiency was found for source distances from 10 to 100 cm. It is well known that the counting rate does affect the peak shape, increasing the width through pile-up in the main amplifier. This effect is discussed by Fairstein and Hahn[39]. To insure consistency in different measurements, all spectra were recorded at 20% dead time on the analyzer. The singles counting rate at this dead time is 10^3 - 10^4 counts/sec. It was felt that counting for a fixed dead time is better than counting at fixed counting rate for the following reason. The undershoot for high energy pulse is greater than for low energy ones, but the analyzing time is also greater. Thus the effect of the larger under-shoot is compensated by the longer dead time and smaller counting

rate. A second fixed range of the spectrum was used for lines with energies up to 2.5 MeV.

The following sources were used in fitting the peak shape parameters (energies taken from Ref. 34):

^{241}Am(59.5 keV), ^{170}Tm(84.3), ^{57}Co(121.9), ^{141}Ce(145.4), ^{114}Cd(191.6), ^{203}Hg(279.1), ^{7}Be(477.4), ^{137}Cs(661.6), ^{54}Mn(835.3), ^{46}Sc(1120.5), ^{22}Na(1274.6), ^{60}Co(1332.5), ^{88}Y(1836.1), ^{228}Th(2614.5) and ^{24}Na(2753.9).

The polynomial functions used to fix the parameters in the function F are as follows:

B(area parameter) = ATAIL = 0.035/CH + 0.039 - 0.012 * CH + 0.0054 * CH^2

λ_1 = EL = 0.719 + 0.296 + CH + 0.0274 * CH^2

$2\sigma\sqrt{2\ln 2}$ = FWHM = SQRT (12.03 + 2.168 * CH)

λ_3 = ET = 33.55 - 6.08 * CH + 0.395 * CH^2

λ_2 = EH = 0.85 + 0.24 * CH CH = channel number

A plot of the parameters is shown in Figure 4. An example of the fitting program is given in Figure 3, with the fitted parameters in Table 2.

5. Efficiency Calibration

After the parameters were fixed, the efficiency calibration was made. The sources used are given in Table 3. At high energies, the efficiency varies slowly. At lower energies, there is more variation and more points are necessary. In finding

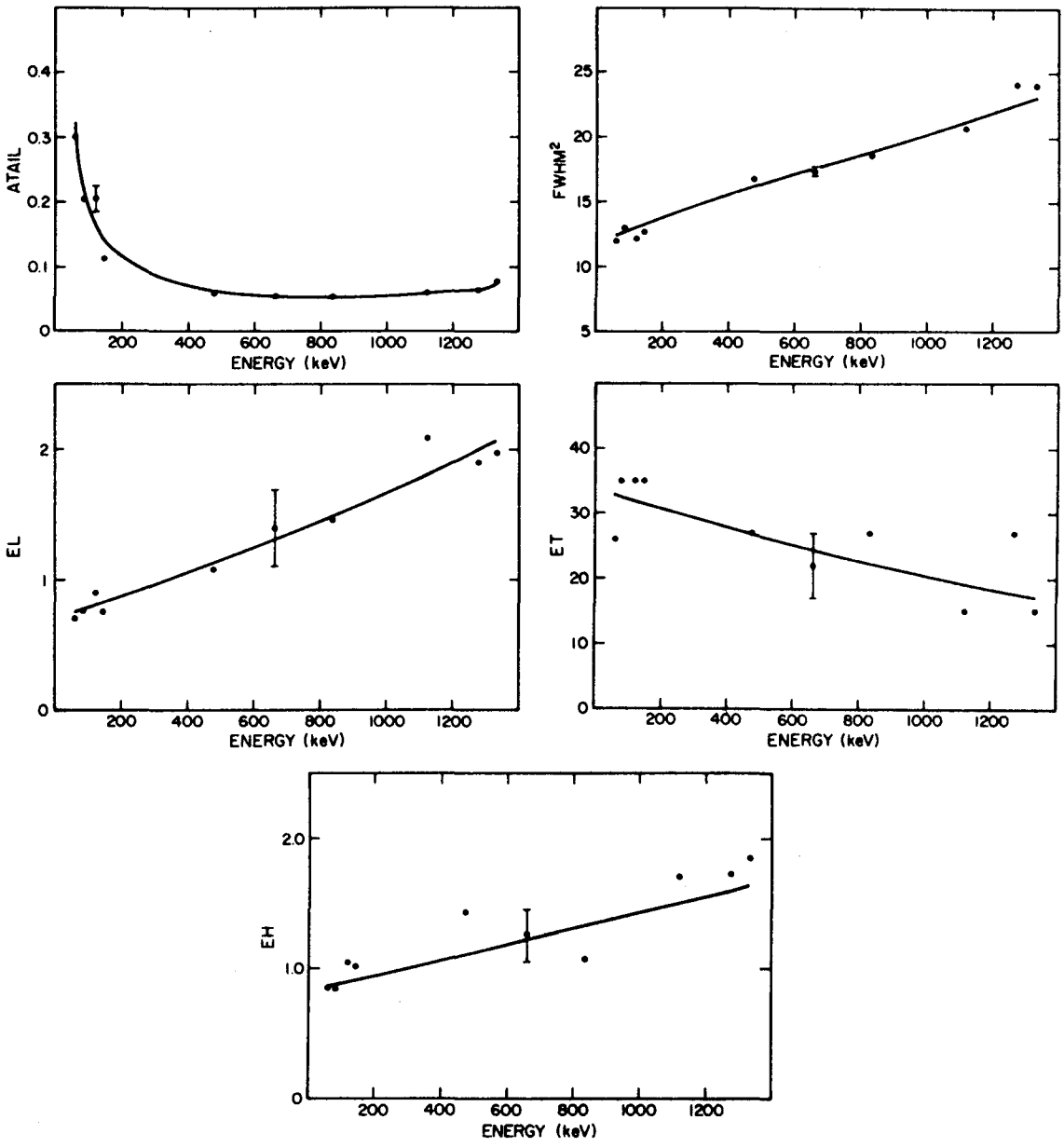

Figure 4

Fixed parameters in the function F. The solid curve is the least squares fit.

Table 2

Fitted Lines in ^{154}Gd

	1241.6, 1246.6 keV		1274.4 keV	
Parameter	Value	Standard Error	Value	Standard Error
a	$.2045 \times 10^{4}$	$.22 \times 10^{2}$	$.1091 \times 10^{4}$	$.11 \times 10^{3}$
b	$.9563 \times 10^{1}$	.54	$.3219 \times 10^{1}$	$.21 \times 10^{1}$
c	.2313	$.43 \times 10^{-1}$	$-.3024 \times 10^{-1}$	.12
A_1	$.5967 \times 10^{4}$	$.32 \times 10^{3}$	$.1351 \times 10^{7}$	$.10 \times 10^{5}$
x_0	$.2711 \times 10^{2}$	$.50 \times 10^{-1}$	$.4400 \times 10^{2}$	$.71 \times 10^{-2}$
A_2	$.3533 \times 10^{5}$	$.40 \times 10^{3}$		
x_0	$.3996 \times 10^{2}$	$.11 \times 10^{-1}$		
	SE = 1.2		SE = 8.7	

The standard errors are given by the values of the error matrix multiplied by SE. SE is equal to $\sqrt{\chi^2/(n-m)}$.

suitable sources, the most difficult problem is in connecting the region above and below 500 keV; above this energy there are nuclei with cascade transitions, below there are accurate bent crystal measurements. ^{22}Na was not used because the 511 keV annihilation peak is noticeably wider than calibration lines of the same energy and would not be fitted properly with the fixed parameters.

The form of the efficiency curve has been quoted[39] as a semi-empirical relation $EFF = D/c[1 - \exp(-\tau c) + A\sigma \exp(-BE)]$

$E = \gamma$-ray energy, c = thickness of crystal

τ = photoelectric cross section A, B, D = empirical constants

σ = Compton cross section.

For high energies, τc is small and we can write

$$EFF = D[\tau + A\sigma \exp(-BE)]$$

At high energies, τ and σ vary slowly with energy. This suggests fitting the efficiency to an exponential in powers of the energy.

A linear least-squares fit was made therefore, to the expansion

$$\log EFF = \log A + a + bE + cE^2 + dE^3 + \ldots$$

The $\log A_i$ term provides a parameter for normalization for each different source used in the fit, since it shifts the points up or

Table 3

Relative Intensity of Lines used in Efficiency Calibration

Source	Gamma Ray Energy	Relative Intensity	Source	Gamma Ray Energy	Relative Intensity
^{60}Co	1332.5	1.00[35]	^{169}Tm	307.7	28[37]
	1173.2	1.00		261.0	4.8
				198.0	100
^{46}Sc	1120.5	1.00[35]		177.2	62
	889.3	1.00		130.5	31
				118.2	5.2
^{154}Eu	1274.4	33.5[36]		109.8	50
	1004.8	17.3		93.6	7.2
	996.3	10.3		63.1	121
	873.2	11.5		Errors 5%	
	723.3	19.7			
	591.7	4.84			
	444.4	0.50 (5%)	^{182}W	264.1	26.9(12)[38]
	248.0	6.59		229.3	27.7(12)
	188.2	0.228 (5%)		222.0	56.1(22)
	123.1	40.5		198.3	10.7(6)
	Error 2% except where noted			179.4	22.9(10)
				156.4	20.0(9)
				152.4	51.0(20)
^{166}Er	829.7	12.9(3)[1]		116.4	3.16(19)
	809.5	76.4(8)		113.7	13.6(7)
	751.5	15.2(3)		100.1	100
	710.6	71.5(7)		84.7	18.8(9)
	529.1	13.0(4)			
	410.5	16.8(2)	^{114}Cd		
	279.6	43.6(4)		725.2	1.00[35]
	215.6	4.15(6)		558.5	1.00

down so that they lie on the best polynomial. The coefficients a, b, c, ... determine the polynomial and are the same for all sources. The total number of parameters is (n + 1) for the polynomial E^n, plus one additional parameter for each source used. The region below 100 keV was not fitted; the efficiency drops off sharply due to absorption in the dead layer of the detector, and there were not enough sources to measure the efficiencies accurately. The efficiency curve is shown in Figure 5. The errors in the calibration are 2% in the region 1300 to 500 keV, with an additional 0.5% per 100 keV from 500 to 100 keV. The relative efficiency, however, in a limited region of energy is better than 0.2% per 100 keV.

6. Energy Calibration

The energy calibration was made by simultaneously recording the spectrum of the isotope under study with several calibration isotopes whose energies were well known. The position of the reference lines was determined by the fitting program, and a fit of the energy as a polynomial function of channel number was made. The coefficients of this polynomial were then used to determine the energy of the lines under study. The errors in the peak positions given by the fitting program are of the order of 0.05 channel, but the nonlinearities of the system limited the

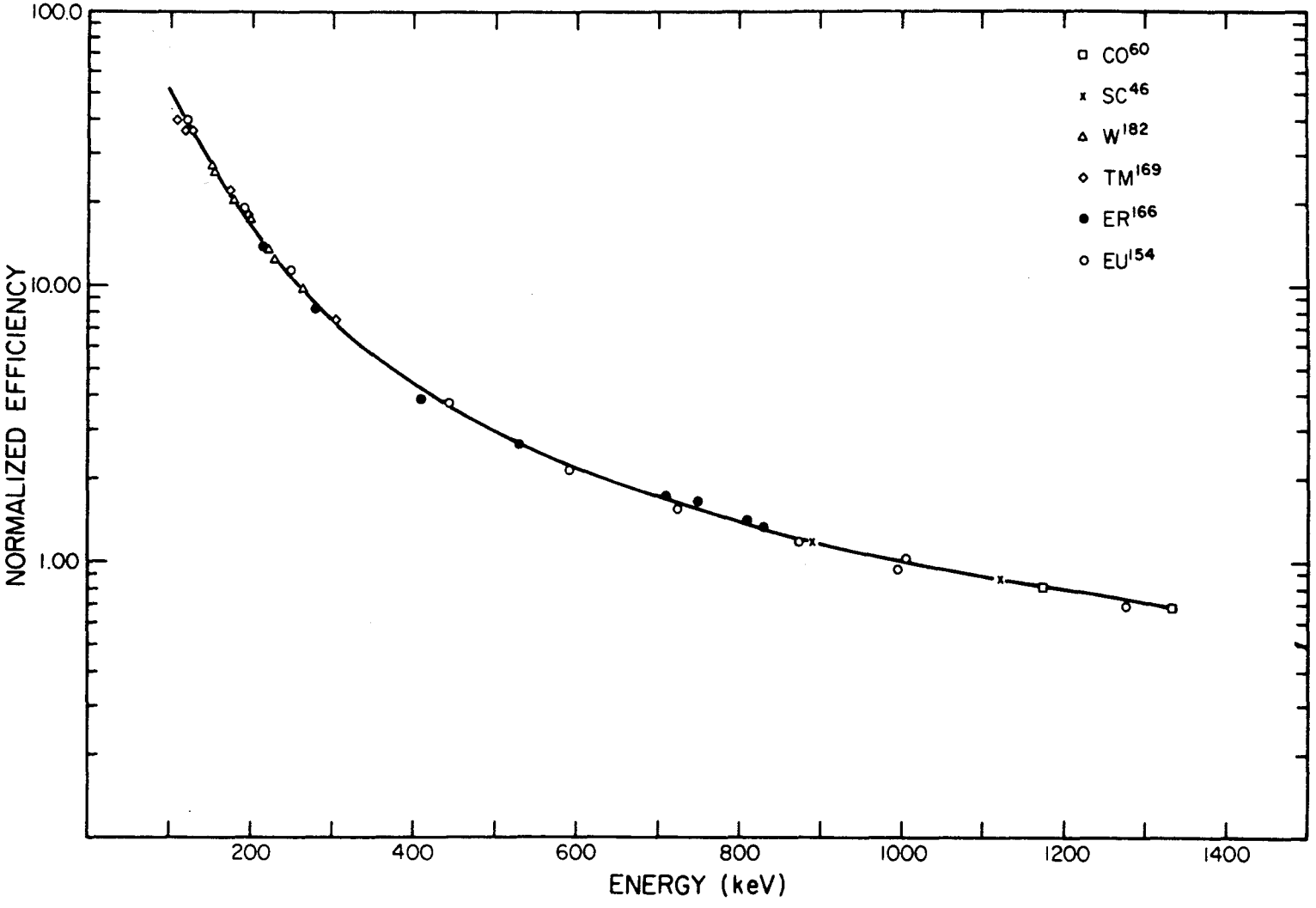

Figure 5

Intrinsic relative full energy peak efficiency curve for the 5 cm^2 x 10 mm Ge(Li) detector.

accuracy of the measured energies to 0.1 keV.

7. Conclusion

There are several advantages in the peak fitting program described here over previous methods. The function used gives a better fit to the experimental full energy peak shape, especially for strong peaks with more than 10^5 counts in height, than the commonly used Gaussian. The fit is often better by a factor of 5-10 in the quantity $X^2/(n-m)$. The fit may be even better than our values of $X^2/(n-m)$, which is based on statistical error in our data, since the analyzer used had an even-odd effect in adjacent channels, and the scatter of the points was considerably greater than statistical. Calibration sources are fitted in the same way as peaks of unknown spectra, so that any difference between the function and actual shapes are minimized. In fitting peaks with multiple components, fixing all parameters except position and area removes large correlations between parameters and insures a better fit. The least squares program handles large numbers of parameters efficiently, and all information on correlations and errors can be printed out. Energies are given to better than 0.1 keV, depending on the linearity of the system and the number of calibration sources used. The relative full energy peak efficiency of the 5 cm^2 x 10 mm Ge(Li) detector has been

measured using sources with accurately measured intensities. Intensities of gamma rays under investigation are determined to better than 5%. In a narrow energy interval of 100 keV in the region between 500 and 1300 keV, the relative intensities can be obtained with an accuracy of better than 0.2%.

C. Source Preparation

Levels of ^{152}Sm, ^{152}Gd, and ^{154}Gd are populated in the radioactive decay of ^{152}Eu and ^{154}Eu, as obtained by neutron irradiation with the Materials Testing Reactor at Arco, Idaho. ^{152}Eu ($\tau_{1/2}$ = 12 y) and ^{152}*Eu($\tau_{1/2}$ = 9.3h) were prepared by irradiation of enriched ^{151}Eu. For the former, the source was approximately one year old at the time of study, while in the latter case experiments were begun 18 hours after the end of the neutron irradiation. A contamination of ^{154}Eu made corrections in the intensities of some lines in ^{152}Sm necessary. The ^{154}Eu ($\tau_{1/2}$ = 16 y) source was prepared by irradiation of enriched ^{153}Eu and was approximately two years old at the time of study. The only contamination observed was attributed to ^{155}Eu. The source for the angular correlation experiments was prepared by dissolving the active europium oxide in dilute HCl. The source holder was a lucite cylinder, inside dimensions 3mm diameter by 8mm height. The internal conversion spectrum of ^{154}Eu was

measured as a calibration for the Si(Li) detector on the 35 cm radium $\pi\sqrt{2}$ iron free spectrometer. The source was made by evaporating Eu Cl in vacuum on an aluminum foil from a tungsten boat, then cutting the foil into a rectangle 2.5 cm x 0.15 cm.

Levels in ^{166}Er are populated in the radioactive decay of Ho 166m (1200 yr). A 20 μc source was purchased from Nuclear Science and Engineering Company, Pittsburgh, Pennsylvania. The only detectable impurity was ^{154}Eu (16 yr).

Levels in ^{232}U are populated in the radioactive decay of ^{232}Pa (1.3 d). Sources were prepared by neutron irradiation of ^{231}Pa (230 barns) at the MTR reactor, Arco, Idaho. The ^{231}Pa was obtained from the AEC loan pool, Oak Ridge. Experiments were begun approximately 18 hours after the irradiation. After ten days, the activities of ^{233}Pa and long lived fission products became appreciable. The electron sources were prepared by dissolving the Pa_2O_3 in HF, placing a drop of the solution on mylar foil wetted with insulin, then drying with a heat lamp. The source material was visible to the eye, and the spot was 0.5 cm in diameter.

A source for the bent-crystal spectrometer was made by filling a quartz capillary 0.2mm in diameter with Pa_2O_3. The material was added to a height of approximately 2.5 cm. The

source was then irradiated at the MTR reactor.

D. Angular Correlation Experiments

The mixing ratios of several gamma to ground state band transitions in ^{154}Gd were determined by measuring their angular correlation with gamma rays of known multipolarity. The experiments were performed using two 7.6 x 7.6 cm NaI(Tl) scintillation spectrometers. The source was a dilute HCl solution of ^{154}Eu (16 y). The pulse height spectrum in one detector in coincidence with the photopeak of a single gamma ray in the other was stored in a pulse height analyzer, each quadrant corresponding to a different angle between the detectors. One detector was fixed; the other was moved automatically to a new angle every 200 seconds. Single counting rates in each detector and triple coincidences from the fast-slow coincidence circuit were printed out after each angle. The angular correlation table and associated electronics have been discussed by Bowman.[40] In this way several angular correlations were measured simultaneously with each of the 123, 248, and 724 keV gamma rays. In the first two cases, contributions due to competing cascades were experimentally determined by measuring the angular correlation with the Compton events just above the 123 and 248 photopeaks. The angular correlation coefficients have been corrected for random

coincidences, finite solid angle,[41] and coincidences with the Compton background.

Several authors have found the angular correlation between the 1274 and 123 keV gamma rays to be attenuated by time dependent perturbations during the 1.70 ns intermediate state lifetime.[8, 41] These perturbations can exist even in a liquid source; an example is the interaction of an electric field gradient with the nuclear quadrupole moment of the excited state. The time-differential measurement of the angular correlation was performed using a 5 x 5 cm NaI(Tl) scintillation crystal coupled to a 56 AVP photomultiplier tube to detect the 1274 keV gamma ray, and a Pb loaded plastic scintillator also mounted on a 56 AVP tube to detect the 123 keV gamma ray. The output of a time to amplitude converter was stored in a multichannel analyzer, again using separate quadrants to correspond to different angles between the detectors. This time spectrum displays the 1.7 ns lifetime of the 2^+ state. A least squares fit of the time dependence of $A_2(t)$ gave $\lambda_2 \tau_{123} \leq 0.05$. We therefore neglected any correction due to intermediate state attenuation in the measured correlation coefficients.

E. The Electron Spectrometer

The measurement of conversion electrons following

nuclear decay can provide further information to the results of gamma ray studies. Transition multipolarities can be determined from absolute K shell conversion coefficients or through L subshell ratios, and electric monopole transitions between 0^+ states can only occur through internal conversion. EO transitions are also possible for transitions from the beta band in deformed nuclei to the ground state band ($\Delta K=0$), between states of equal spin (2-2, 4-4). As a supplement to the Ge(Li) spectrometer for gamma rays, a solid state detector using the same electronics would clearly be useful.

We have constructed an electron spectrometer for the study of beta rays and conversion electrons using a lithium drifted silicon detector. These detectors have several advantages over magnetic electron spectrometers. Detectors of depth greater than 3mm have high efficiency-approximately 100% intrinsic efficiency for electrons of energy less than 1.5 MeV. Data can be accumulated rapidly, since the entire spectrum can be recorded simultaneously. The resolution of the detector is quite adequate; in our spectrometer, the resolution for the K electrons of ^{232}U at 550 keV was 2.5 keV FWHM. At 1 MeV, the resolution was just over 3 keV. The greatest disadvantage of the solid state detectors is the large Compton background

resulting from the scattering of gamma rays.

A drawing of the spectrometer is given in Figure 6. The detector is of commercial manufacture (Simtec) with dimensions 200 mm^2 x 3 mm drifted depth. The detector is mounted on the end of a copper cold finger which remains in contact with liquid nitrogen in a storage dewar. The source is mounted on a movable rod so that the source to detector distance may be varied. There is a source chamber which can be evacuated, so that sources may be changed without disturbing the detector. A commercial absorption pump was used as a roughing pump. The pump contained approximately 2 liters of molecular seive, which, when chilled with liquid nitrogen, captures gases by physical absorption. The pump can evacuate the chamber from atmosphere to a few microns pressure. Originally, a cold-trapped oil diffusion pump was used, but the trapping was not completely effective and small amounts of oil condensed on the detector. This resulted in absorption of electrons in the oil and worsening of the detector resolution. After roughing was completed, a Vac-ion pump was used, which, with the condensing effect the cold finger and cryostat walls, maintained the vacuum.

The electronics used with the detector is similar to that used with the Ge(Li) spectrometer. A Canberra 1408C

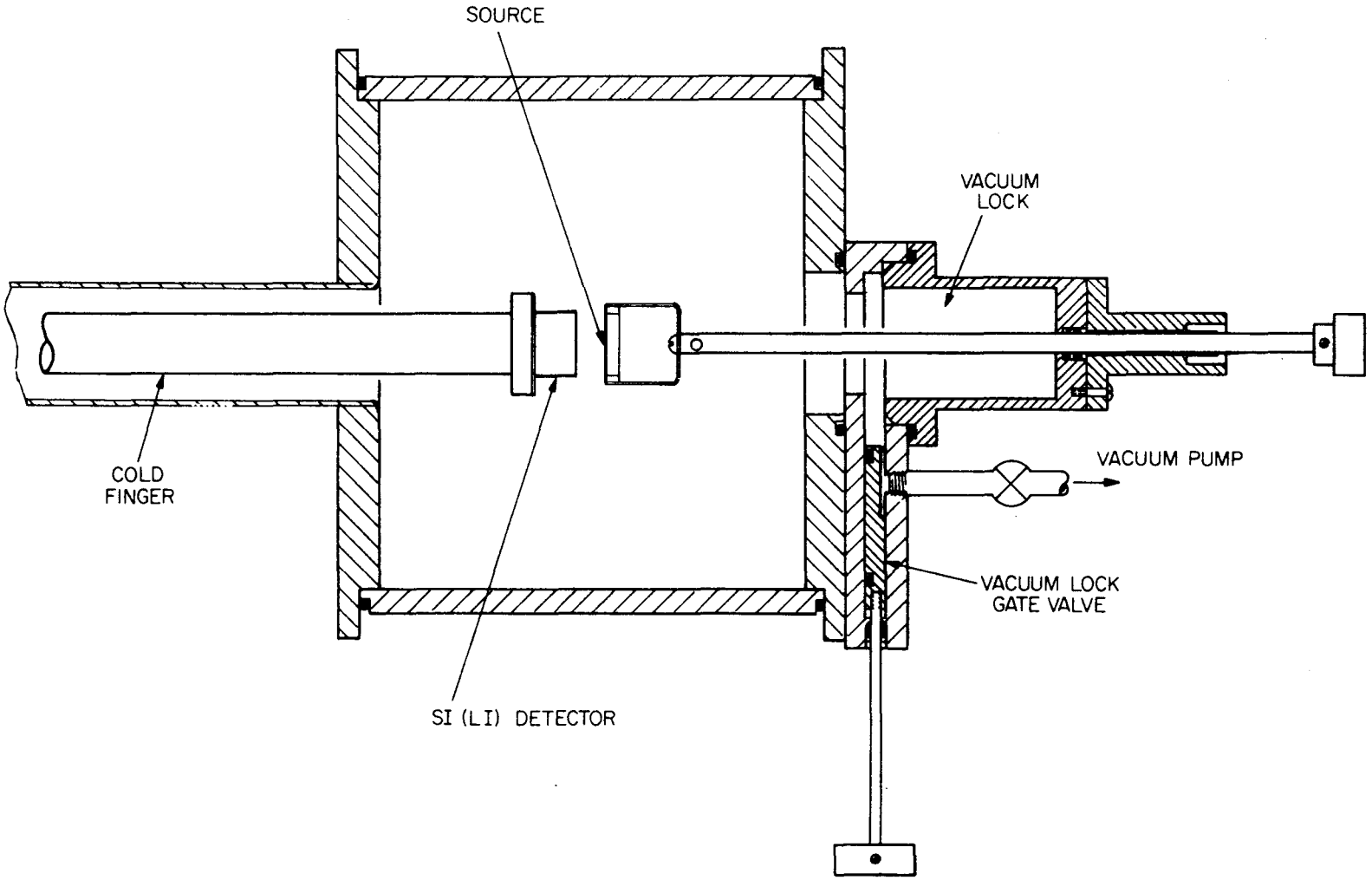

Figure 6

Details of the vacuum chamber of the Si(Li) electron spectrometer.

preamplifier and 1416 amplifier were used. Pulses fed through the preamp were used as reference for the digital stabilizer of the multichannel analyzer. The detector bias voltage was maintained at 600 volts with an Ortec power supply.

The conversion electron line shape is dependent on the thickness of the source used, as the electrons are absorbed in passing through the source material. The peak areas were measured graphically. The detector was calibrated by using conversion electron intensities measured in ^{154}Gd using the 35 cm $\pi\sqrt{2}$ iron free beta spectrometer. The efficiency was found to be 100% ($\pm$ 10%) up to 1.5 MeV.

IV. RESULTS OF DECAY SCHEME STUDIES

A. ^{152}Sm, ^{152}Gd, and ^{154}Gd

^{152}Sm and ^{154}Gd are located in the transition region between spherical vibrational nuclei and the strongly deformed rare-earths. The transition from spherical to deformed nuclei is quite sudden, with ^{152}Gd showing a typical spherical vibrational spectrum and ^{154}Gd exhibiting the rotational levels characteristic of a deformed nucleus. Beta and gamma vibrational bands are populated in ^{152}Sm and ^{154}Gd by radioactive decay of long-lived parents. These two nuclei offer a unique opportunity to study the possible interaction of the two vibrational modes, for as deformation increases in the rare earth nuclei, the beta band is pushed up in energy and has not been identified with certainty in the strongly deformed rare earth nuclei.

1. Gamma-Ray Spectrum of ^{152}Eu ($\tau_{1/2}$ = 12 yr)

A typical gamma-ray spectrum of ^{152}Eu (12 yr) is shown in Figure 7. Three separate measurements were made for the strong lines, the period of data accumulation being about four days. For the weaker lines, each spectrum was analyzed at intermediate points in the run as well. The computer program described in Section B, Chapter II was used to obtain the energies

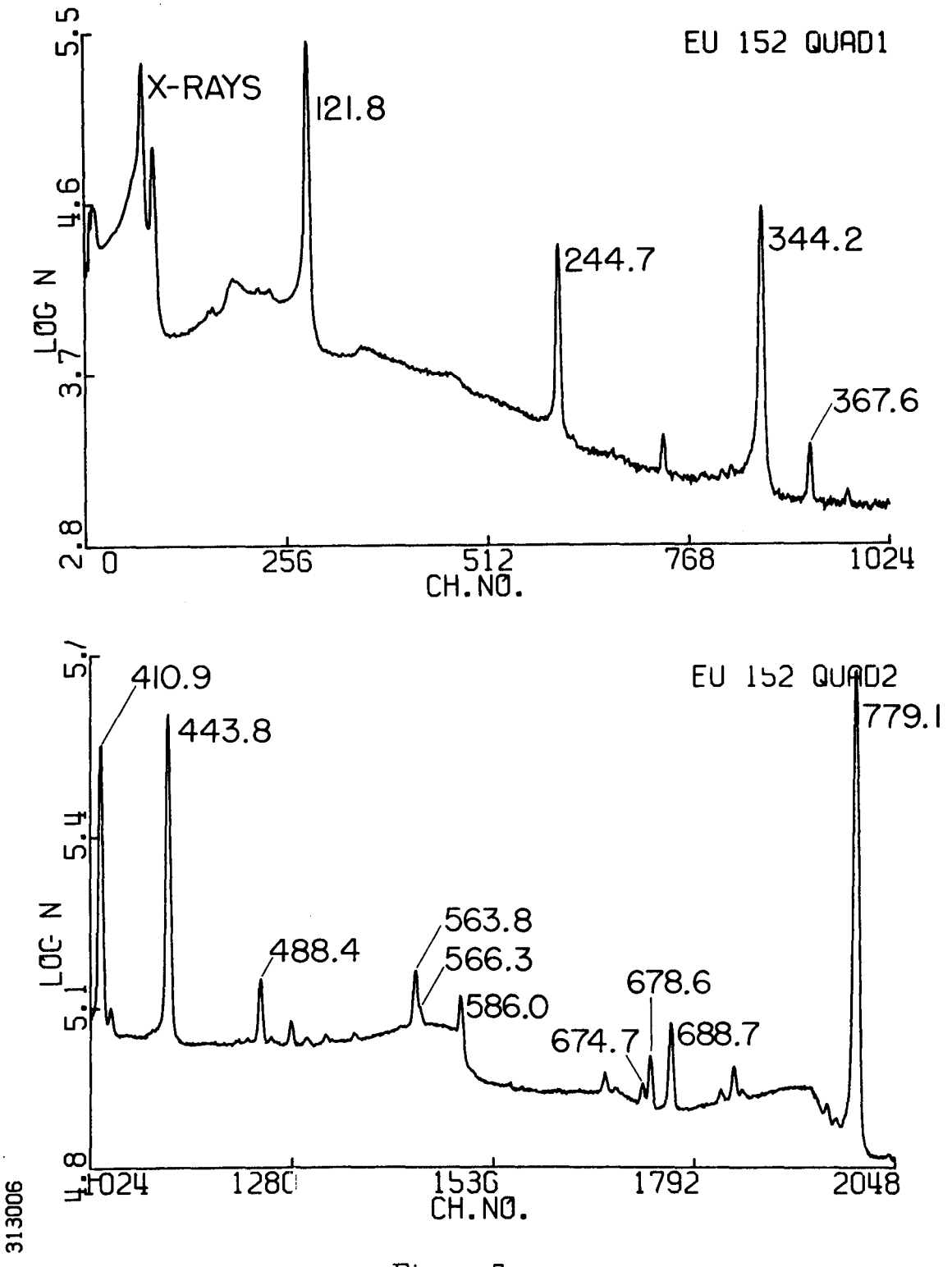

Figure 7a

The gamma ray spectrum of ^{152}Eu. The second, third, and fourth quadrants are taken from a single spectrum. Because of overflow,

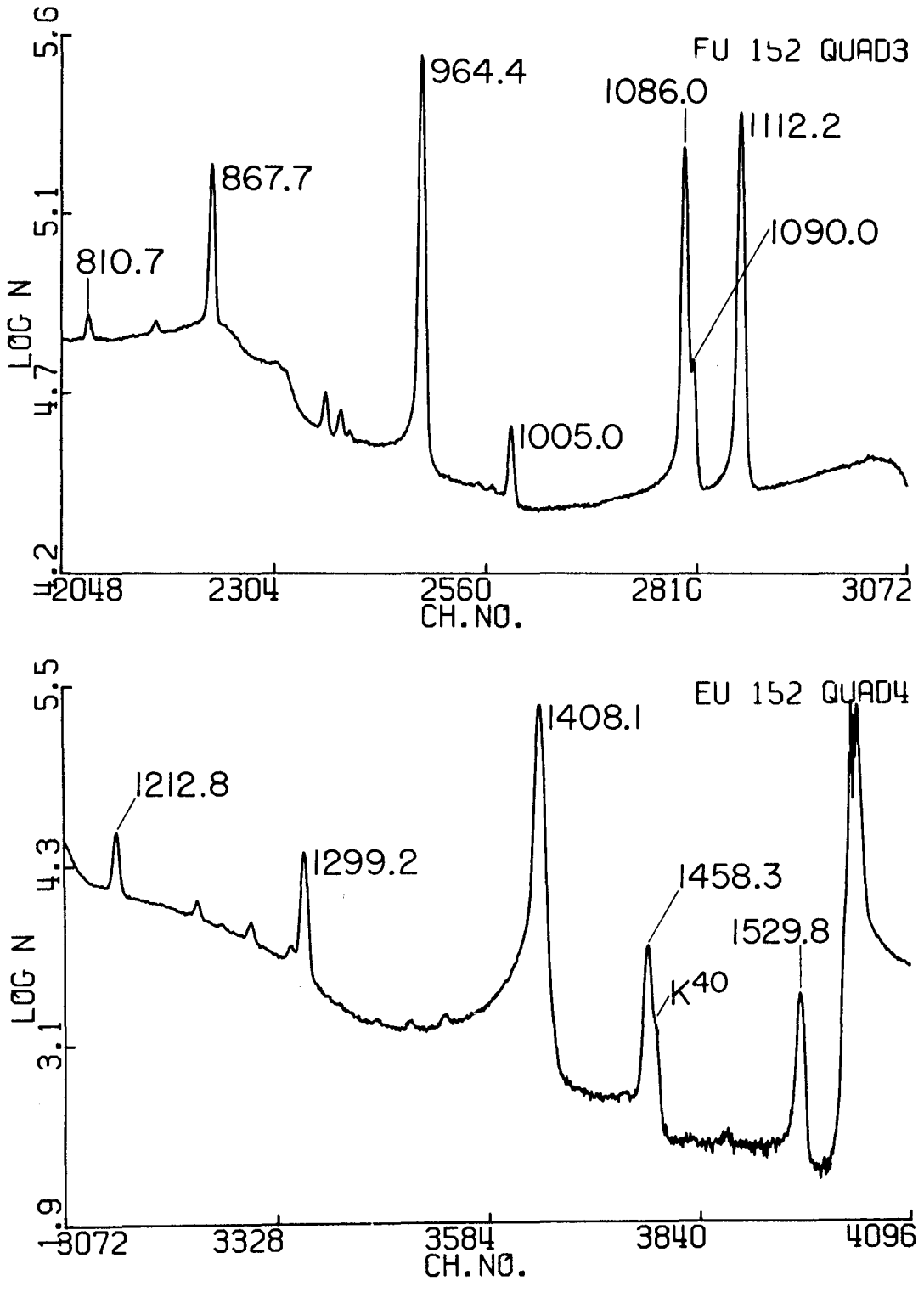

Figure 7b

the first quadrant was recorded for a shorter time. Weak lines in the first quadrant were analyzed from the longer runs.

and intensities given in Table 4, where the results are compared with those of Dzhelepov[42], et al. Of the lines listed, nine lines in ^{152}Sm and five lines in ^{152}Gd have not been reported previously.

2. Gamma-Ray Spectrum of ^{152*}Eu ($\tau_{1/2}$ = 9.3 hr)

The spectrum of the 9.3 hr ^{152*}Eu is shown in Figure 8. Table 5 gives the energies and intensities of lines fed only by the 9.3 hr decay. No attempt was made to accurately determine the amount of feeding when a level was fed by both decays.

3. Level Structure of ^{152}Sm

The decay scheme of ^{152}Sm is shown in Figure 9. Several previously unobserved gamma-rays of the 12 year half-life have been placed in the decay scheme. New lines of 870.1 and 995.8 keV are associated with the 9.3 hour decay. The transition at 444.1 keV cannot be resolved from the stronger 443.8 keV line in the singles spectrum of the 12 yr decay. However, the levels at 1529.9 keV and 810.6 keV are fed differently in the two decays, so the ratio of the two lines to other lines leaving the same level can be found, and the relative intensity of each determined. The line at 444.1 keV can also be measured in coincidence with the 244.7 keV, but the subtraction of Compton and random coincidences gives a larger error than by observing

Table 4

Energies and Relative Intensities of the Gamma Rays in the Decay of 12 year ^{152}Eu

Transitions in ^{152}Sm

Energies (keV)	Relative Intensities This Work	Dzhelepov[42]
121.8	131 (4)	135 (9)
244.7	32.5 (10)	34 (4)
275.4	0.14 (1)	
295.9	1.80 (4)	1.5 (4)
400.5	0.01 (1)	
443.8	11.7 (7)	17.5 (17)
444.1	1.28 (13)	
488.4	1.68 (5)	
493.6	0.12 (3)	
563.8	2.01 (6)	
566.3	0.50 (3)	3.5 (8)
656.5	0.62 (3)	
674.7	0.73 (7)	
688.7	3.41 (7)	3.5 (8)
719.4	1.34 (5)	1.3 (2)
769.2	0.29 (2)	
810.7	1.31 (4)	1.31 (24)
841.8	0.65 (3)	1.00 (8)
867.7	16.8 (2)	16.5 (8)
901.0	0.34 (17)	
919.7	1.68 (4)	2.7 (5)
964.4	59.1 (12)	59.4 (24)
1005.0	2.59 (15)	2.4 (4)
1086.0	41.2 (6)	43.5 (16)
1112.2	55.2 (6)	55.0 (24)
1212.8	5.76 (20)	5.8 (5)
1249.7	0.73 (4)	0.90 (17)
1408.1	85.2 (20)	87.3
1458.3	2.03 (10)	1.8 (2)
1529.8	1.4 (1)	1.0 (5)

Transitions in ^{152}Gd

Energies (keV)	Relative Intensities	
	This Work	Dzhelepov[42]
271.0	0.30 (2)	
344.2	112.2 (3)	123 (5)
367.6	3.55 (10)	4.4 (2)
410.9	9.29 (18)	9.6 (10)
503.3	0.62 (2)	
586.0	1.93 (6)	1.75 (80)
678.6	1.92 (12)	
712.9	0.37 (3)	
779.1	52.4 (5)	52.4 (25)
930.8	0.32 (3)	
1090.0	6.84 (24)	7.0 (17)
1299.2	6.64 (50)	6.8 (4)

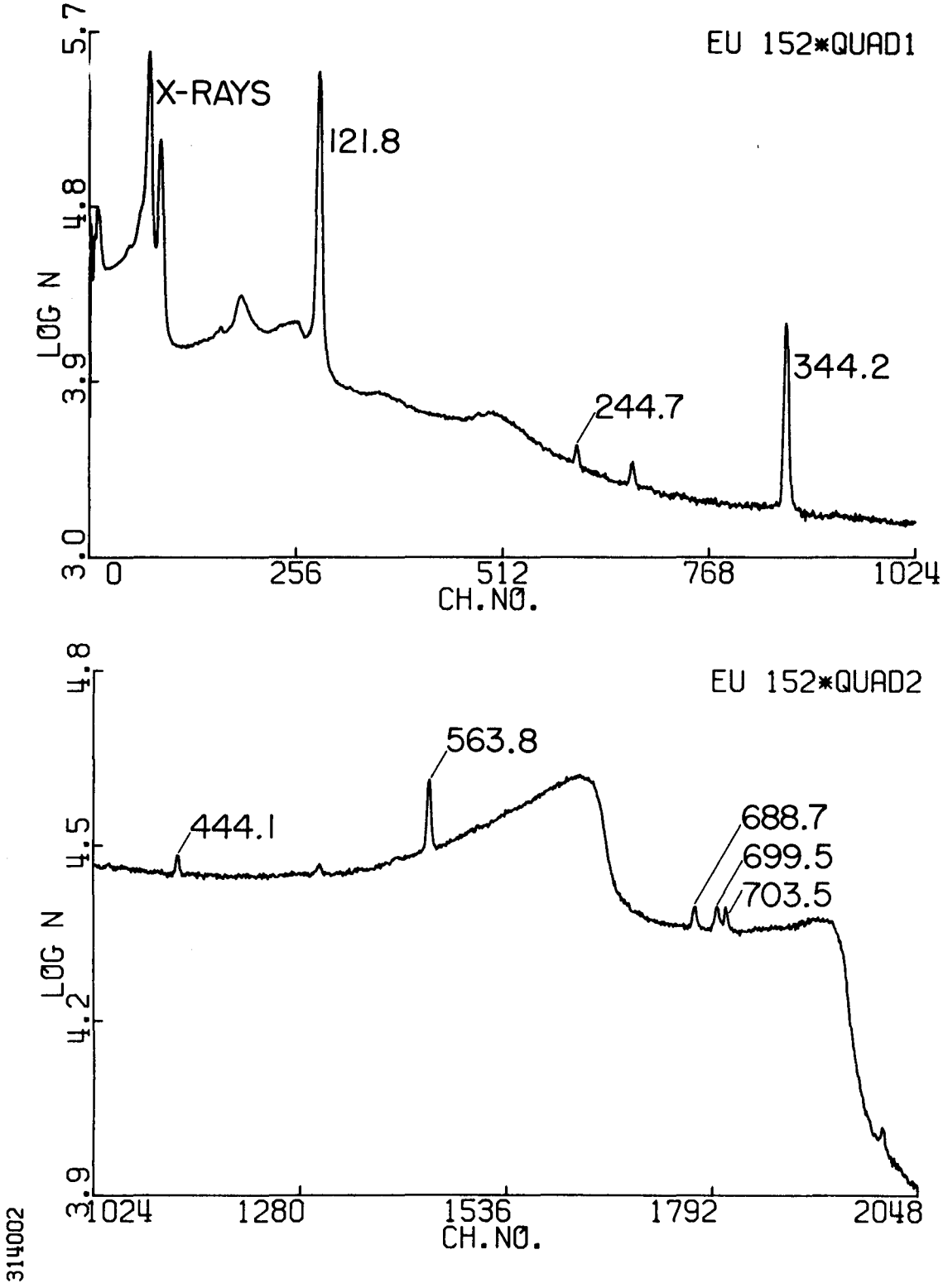

Figure 8a

The gamma ray spectrum of ^{152*}Eu.

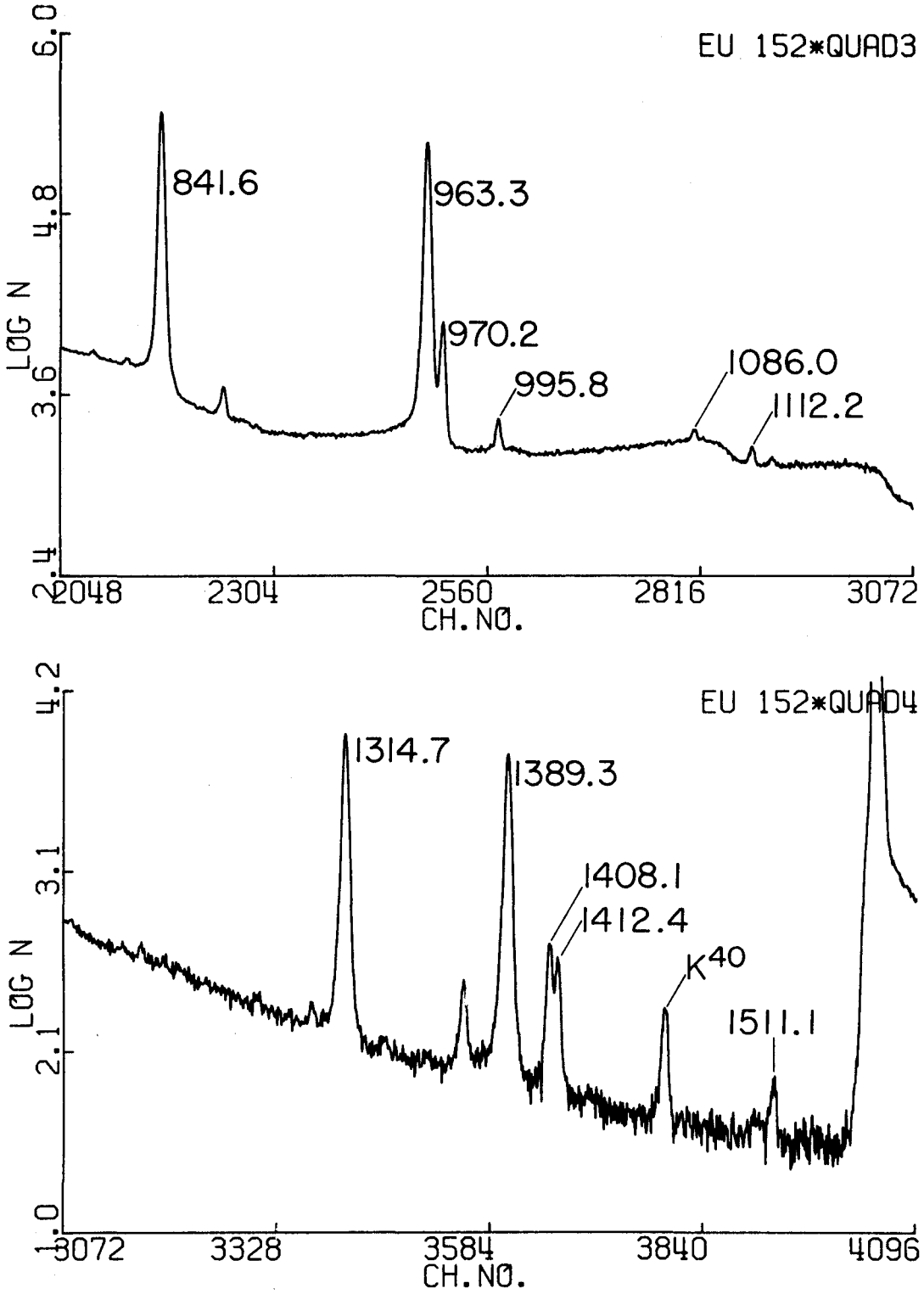
EU 152*QUAD3
841.6
963.3
970.2
995.8
1086.0
1112.2
LOG N
6.0
4.8
3.6
2.4
2048
2304
2560
2816
3072
CH. NO.
EU 152*QUAD4
1314.7
1389.3
1408.1
1412.4
K40
1511.1
LOG N
4.2
3.1
2.1
1.0
3072
3328
3584
3840
4096
CH. NO.

Figure 8b

Table 5

Energies and relative intensities of Gamma Rays in the Decay of 9.3 hr ^{152}Eu

Transitions in ^{152}Sm

Energies (keV)	Relative Intensities This Work	Dzhelepov[43]
703.5	0.28 (2)	
841.6	65.2 (6)	65 (10)
870.1	0.40 (3)	
963.3	53.9 (5)	54 (5)
995.8	0.30 (2)	
1389.3	3.57 (12)	3.4 (4)
1412.4	0.195 (10)	0.16 (5)
1511.1	0.028 (7)	0.03
1560		0.03
1680		0.03

Transitions in ^{152}Gd

Energies (kev)	Relative Intensities This Work	Dzehelepov[43]
699.5	0.34 (2)	0.3 (2)
970.2	2.45 (5)	3.8 (12)
1314.7	4.14 (12)	4.3 (5)

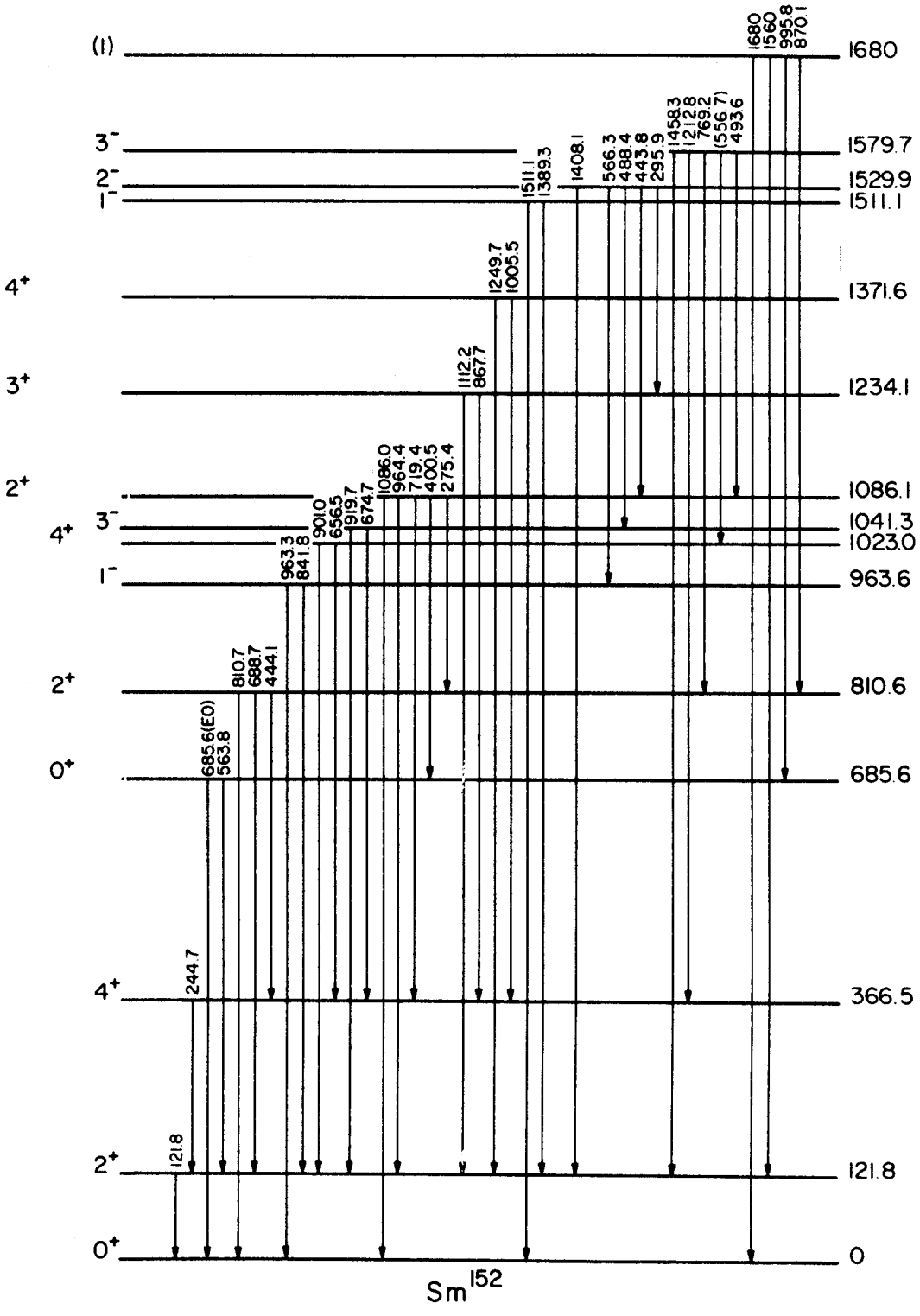

Figure 9

The decay scheme of ^{152}Sm.

the two decays.

a. Ground state band.

The 0^+, 2^+, 4^+ members of the ground state band occur at 0 , 121.8, and 366.5 keV. The 6^+ level reported by Veje, et al[44] at 705 keV is not fed sufficiently to be seen.

b. Beta vibrational band.

The 0^+, 2^+, 4^+ members of the beta-vibrational band occur at 685.6, 810.6, and 1023.0 keV. The assignment of the 4^+ level follows inelastic scattering measurements[44] which assign the 1041 level as the 3^- state of the octupole band.

c. Gamma-vibrational band.

The members of the gamma-vibrational band 2^+, 3^+, and 4^+ are placed at 1086.1, 1234.1, and 1371.6 keV.

d. Negative parity bands.

The 1^- and 3^- members of a $K^\pi = 0^-$ octupole band occur at 963.6 and 1041.3 keV. A 5^- level reported[44] at 1222 keV has not been observed. The reduced branching ratios, assuming the transitions to be pure E1, are given in Table 6. There is good agreement with the strong coupling model for both levels.

The levels at 1511.1, 1529.9, and 1579.7 keV have been identified as the 1^-, 2^-, 3^- members of the $K^\pi = 1^-$ band,[11] but several discrepancies are revealed by the gamma-ray studies.

Table 6

Comparison of Experimental and Theoretical B(E1) Ratios for Negative Parity States in ^{152}Sm

Band	Transition		Energy	Relative B(E1)	Theoretical strong-coupling ratios	
					$K_i = 0$	
$K^\pi = 0^-$	1^-	0^+	963.3	0.55 (1)	0.50	
	1^-	2^+	841.6	1.00	1.00	
	3^-	2^+	674.7	1.10 (4)	0.75	
	3^-	4^+	919.7	1.00	1.00	
Proposed					$K_i = 1$	$K_i = 0$
$K^\pi = 1^-$	1^-	0^+	1511.1	0.006(2)	2.00	0.50
	1^-	2^+	1389.3	1.00	1.00	1.00
					$K_i = 1$	$K_i = 2$
	2^-	2^+_γ	443.8	2.1 (2)	0.5	2.0
	2^-	3^+_γ	295.9	1.0	1.0	1.0
					$K_i = 1$	$K_i = 0$
	3^-	$2^+_{G.S.}$	1458.3	0.18 (1)	1.33	0.75
	3^-	$4^+_{G.S.}$	1212.8	1.00	1.00	1.00

Branching to ground state, beta and gamma bands

Transition		Energy	Relative B(E1)
2^-	$2^+_{G.S.}$	1408.1	1.0
2^-	2^+_γ	443.8	5.0 (3)
3^-	$2^+_{G.S.}$	1458.3	0.6 (2)
3^-	2^+_β	769.1	0.6 (2)
3^-	2^+_γ	493.6	1.0

First, there is strong mixing as evidenced by the energy spacing of the band. The rotational model value for the ($1^- \rightarrow 0^+ / 1^- \rightarrow 2^+$) E1 reduced branching ratio is 2, whereas the experimental value is 0.006, a hindrance of 300. The branching of the 2^- level to the gamma band is in good agreement with K = 2, although the large ft value had led to an assignment of K = 1.[45] Also, the branching is stronger to the K = 2 band than to the K = 0 band. The branching of the 3^- level to the ground-state band does not agree with either K = 0 or 1.

4. Levels in ^{152}Gd

The decay scheme of ^{152}Gd is shown in Figure 10. Previously unreported gamma rays of energy 271.0, 503.3, 712.9, and 930.8 keV have been placed in the decay schemes. The level structure indicates a spherical vibrational nucleus. Reduced branching ratios for levels in ^{152}Gd are shown in Table 7. The 2^+ level at 930.6 keV may be described as a two phonon state, the relative B(E2) value to the one phonon 2^+ level being about 50 times that to the ground state. The transition to deformed shape is quite sudden, with the addition of two neutrons resulting in the well-deformed nucleus ^{154}Gd.

5. Gamma-Ray Spectrum of ^{154}Eu (τ 1/2 = 16 yr)

The gamma-ray spectrum following the decay of ^{154}Eu

Table 7

Reduced Branching Ratios for Transitions in ^{152}Gd

Level	I	Transition		Energy		Reduced Branching Ratio
930.6	2^+	2^+	0^+	930.8	(E2)	2
		2^+	2^+	586.3		100 (10)
1123.3	3^-	3^-	2^+	779.1	(E1)	1.5(1)
		3^-	4^+	367.6		1.0
1314.7	1^-	1^-	0^+	1314.7	(E1)	1.5(1)
		1^-	2^+	970.1		1
1643.	2^-	2^-	2^+	1299.2	(E1)	3 (1)
		2^-	2^+	712.9		1

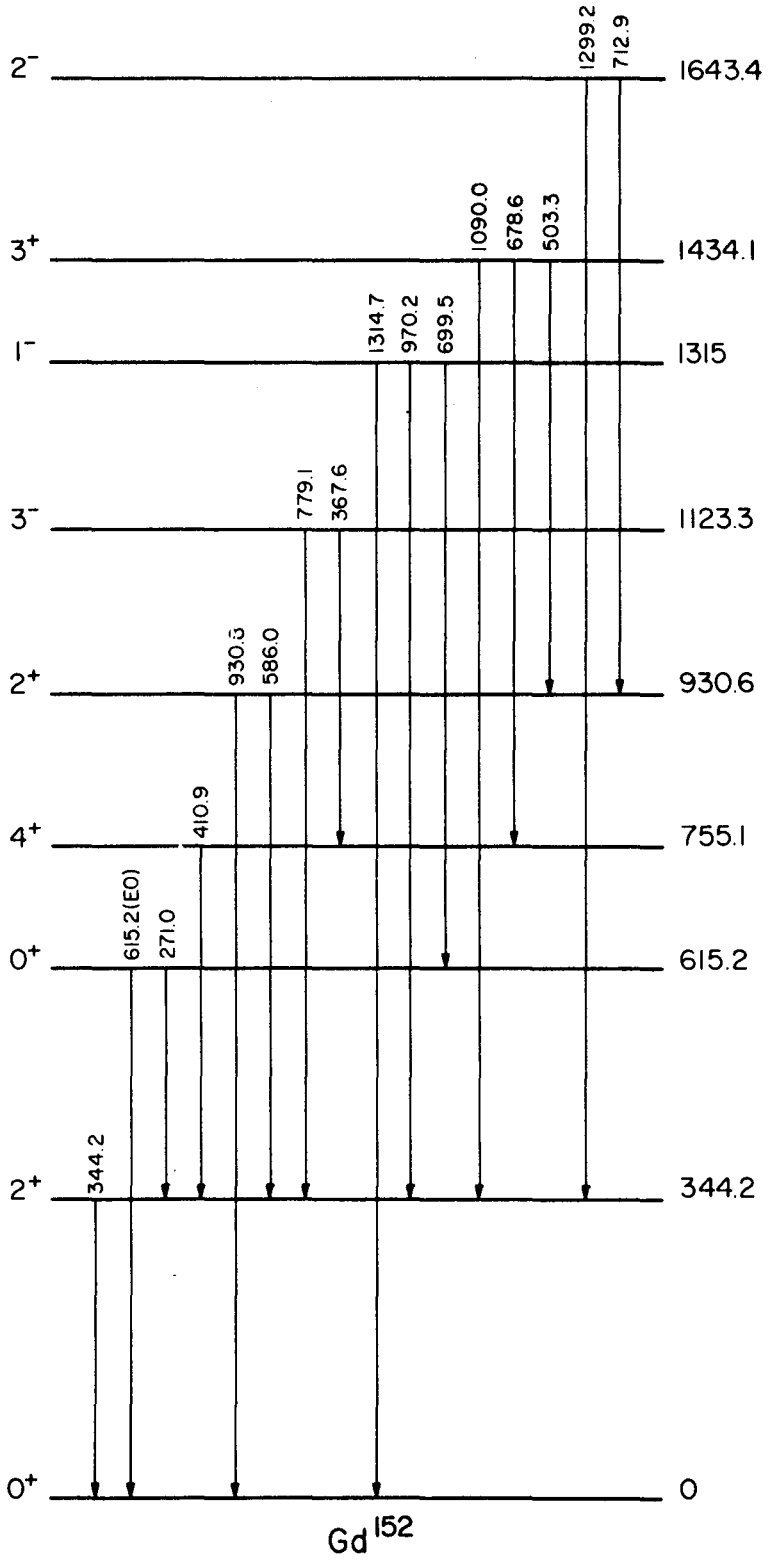

Figure 10

The decay scheme of ^{152}Gd.

is shown in Figure 11. Table 8 shows the energies and intensities of the observed lines. The results are compared with the extensive work of Meyer.[46]

6. Level Structure of ^{154}Gd

Figure 12, following Meyer, shows the band structure of ^{154}Gd.[46]

a. Ground state band.

The 0^+, 2^+, 4^+, and 6^+ members of the ground state band occur at 0 , 123.1, 371.2, and 718.0 keV.

b. Beta vibrational band.

The 0^+, 2^+, and 4^+ members of the beta vibrational band occur at 680.7, 815.6, and 1047.6 keV.

c. Gamma vibrational band.

The 2^+, 3^+, and 4^+ members of the gamma vibrational band are placed at 996.3, 1127.9, and 1263.9 keV.

d. Negative parity bands.

The 0^- octupole band has levels at 1241.3 and 1251.5 keV. The small energy spacing, as well as the lack of agreement of the reduced branching ratios given in Table 8 with the rotational model values, indicates mixing with higher bands.

The proposed $K^\pi = 1^-$ bandhead is at 1509.1 keV. Here the mixing is such that the normal order of the levels is

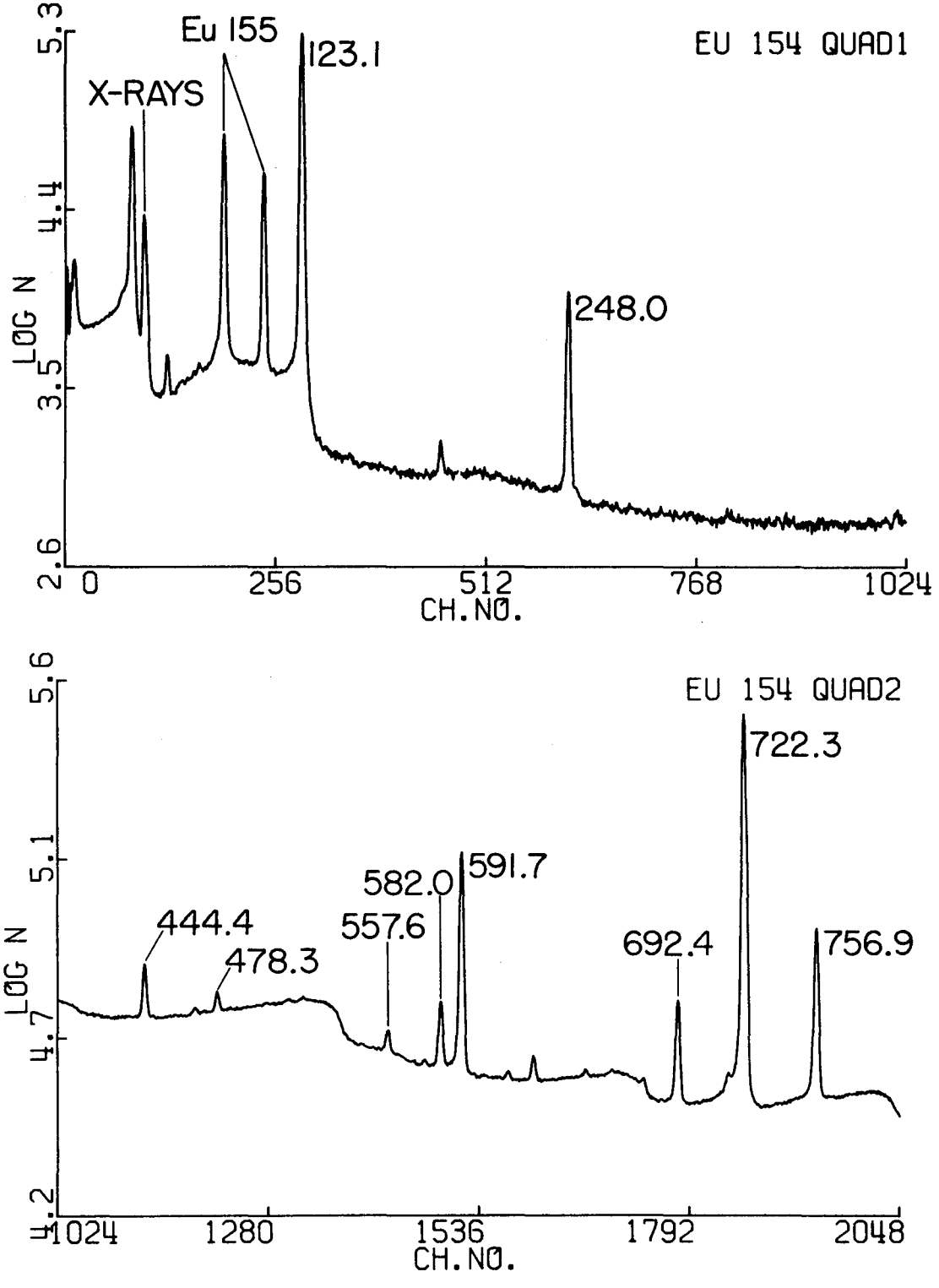

Figure 11a

The gamma ray spectrum of ^{154}Eu.

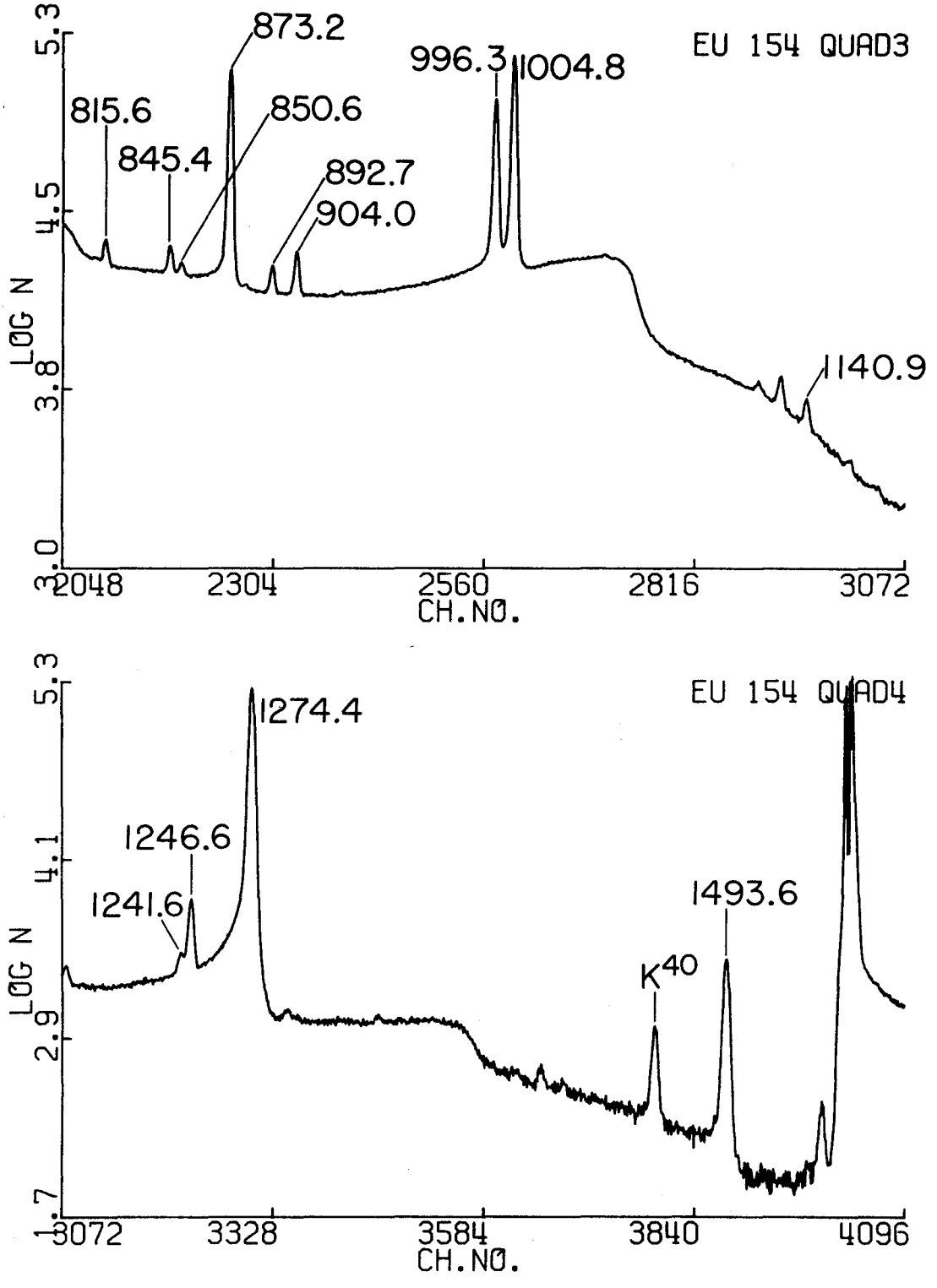
EU 154 QUAD3
873.2
996.3
1004.8
815.6
850.6
845.4
892.7
904.0
1140.9
LOG N
5.3
4.5
3.8
3.0
2048
2304
2560
2816
3072
CH.NO.
EU 154 QUAD4
1274.4
1246.6
1241.6
1493.6
K40
LOG N
5.3
4.1
2.9
1.7
3072
3328
3584
3840
4096
CH.NO.

Figure 11b

Table 8

Energies and Relative Intensities of the Gamma Rays in the Decay of 16 year ^{154}Eu

Energies	Relative Intensities This Work	Meyer[46]*
123.1		40.5
180.7	0.002(2)	0.0045
188.2	0.240(5)	0.228
248.0		6.59
305.1	0.020(4)	0.018
312.3	0.019(4)	0.015
315.4	0.013(4)	0.005
322.0	0.067(3)	0.067
397.1	0.023(3)	0.030
401.3	0.19 (1)	0.21
444.4	0.57 (1)	0.50
467.9	0.060(6)	0.057
478.3	0.210(7)	0.22
512.0	0.032(7)	$\leq$0.042
518.0	0.050(9)	0.047
545.6	0.012(10)	0.017
557.6	0.26 (1)	0.25
582.0	0.91 (2)	0.84
591.7	5.01 (8)	4.84
613.3	0.100(7)	0.093
625.2	0.32 (1)	0.31
676.6	0.15 (1)	0.14
692.4	1.76 (4)	1.70
715.8	0.14 (2)	0.18
722.3	19.6 (3)	19.7
756.9	4.41 (5)	4.34
815.6	0.48 (2)	0.46
845.4	0.56 (2)	0.55
850.6	0.23 (1)	0.23
873.2	11.7 (2)	11.5
880.6	0.05 (2)	0.08
892.7	0.49 (1)	0.46
904.0	0.85 (2)	0.82
924.5	0.06 (1)	0.06
996.3	10.2 (2)	10.3

Energies	Relative Intensities This Work	Meyer[46]
1004.8	17.5 (3)	17.4
1118.5	0.14 (2)	0.10
1128.4	0.31 (2)	0.27
1140.9	0.22 (1)	0.22
1188.6	0.094(3)	0.08
1216.8	-	$\leq$0.004
1241.6	0.15 (1)	0.13
1246.6	0.88 (2)	0.70
1274.4	34.7 (5)	33.5
1387.	0.01	0.020
1408.4	-	0.021
1493.6		0.65
1509.1	0.004	0.005

*Error quoted: 2% for I 1, 5% for 1 I 0.1

Reduced Branching Ratios from Negative Parity Bands[a]

Transition	Energy	Relative B(E1)
1^- 0^+	1241.6	1.00
1^- 2^+	1118.5	1.07(6)
3^- 2^+	1128.4	1.00
3^- 4^+	880.4	0.21(2)
1^- 0^+	1509.1	1.00
1^- 2^+	1386.0	8.00

(a) Meyer, ref. 46

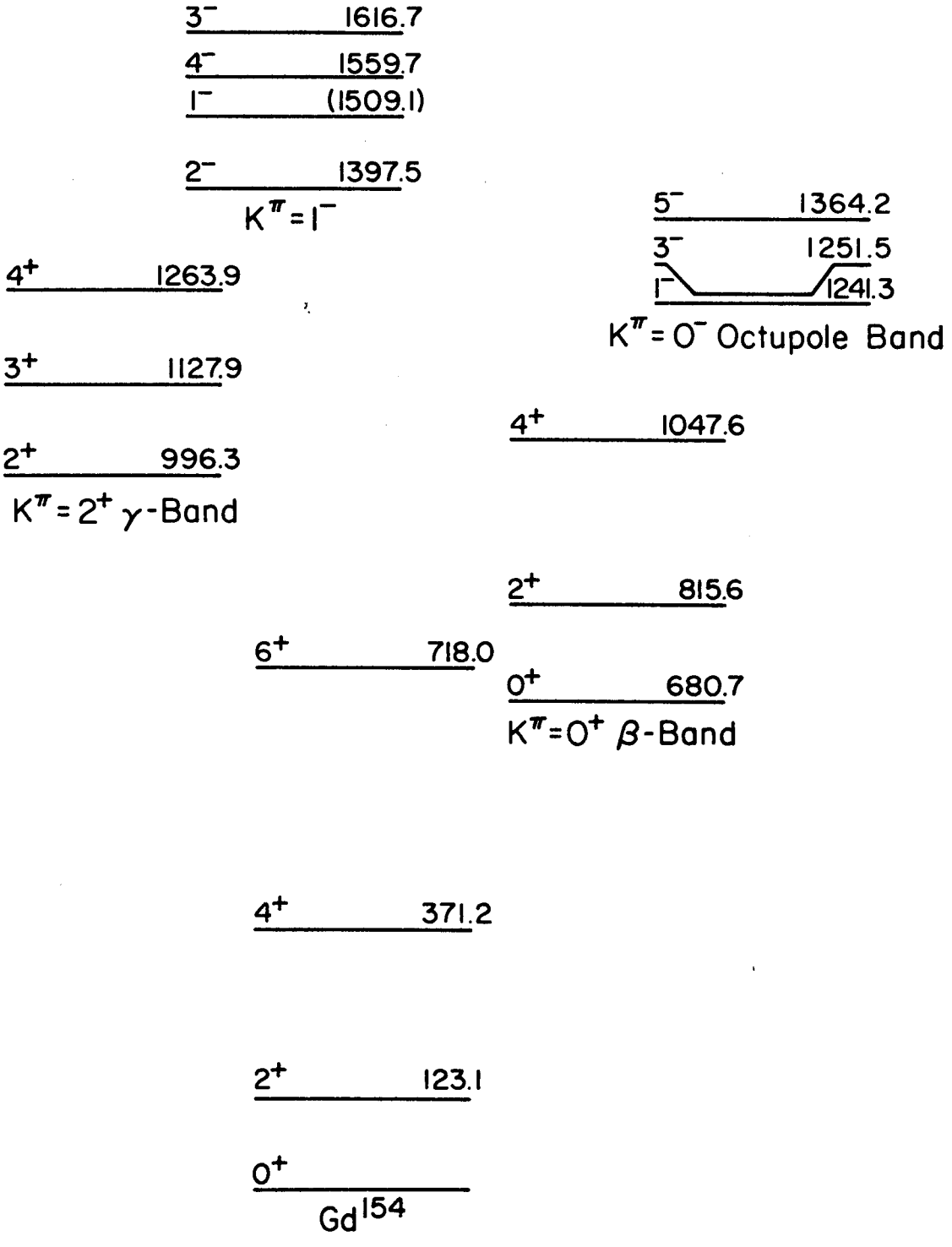

Figure 12

Band structure of ^{154}Gd.

inverted. The strong hindrance observed in ^{152}Sm for the decay of the 1^- level to the ground state does not occur in ^{154}Gd.

7. Angular Correlation Measurements.

The mixing ratios of several gamma to ground state band transitions in ^{154}Gd were determined by measuring their angular correlations with gamma rays of known multipolarity. The experimental techniques are discussed in Section D, Chapter III . A time differential measurement of the angular correlation of the 1274-123 keV cascade was made to measure any attenuation by time-dependent perturbations during the 1.7 ns lifetime of the intermediate state. A least squares fit to the time dependence of $A_2(t)$ gave $\lambda_2 \tau_{123} \lesssim 0.05$. We therefore neglected any corrections due to intermediate state attenuations. The angular correlation coefficients and the mixing amplitudes and ratios deduced from them are shown in Table 9.

B. ^{166}Er

Gunther and Parsignault found agreement with a single z_2 parameter for six branching ratios from the gamma band in ^{166}Er. Their values for the relative intensity of strong lines have errors of only one or two per cent and provide an opportunity to check the results of our peak fitting program. As pointed out in Chapter II, this nucleus offers the best example of the success of

Table 9

Angular Correlation Measurements in ^{154}Gd

	Cascade		Spin Sequence	A_2	A_4	δ Determined from A_2	δ Determined from A_4	%M1
I	873.2	123	$2^+(12)2^+(2)0^+$	-.002(16)	+.303(42)	+ 10.2(18)	$3.5\ ^{+6.4}_{-2.0}$	1% ± .4%
II	1004.8	123	$3^+(12)2^+(2)0^+$	-.205(26)	-.026(50)	$\frac{1}{\delta} = 0 \pm .03$	-	.0 ± .1%
III	1274	123	$2^-(12)2+(2)0+$	+.215(5)	+.007(7)	-.047(5)	-	-
IV	756.9	248	$3^+(12)4^+(2)2^+$	+.179(13)	-.154(21)	4.9(3)	2.3(9)	4% ± 1%
V	892.7	248	$4^+(12)4^+(2)2^+$	+.003(28)	+.098(98)	3.0(10)		10% ± 6%
VI	724.	873	$2^-(12)2^+(12)2^+$	-.126(16)	.000(2)	-5.0(10)		4% ± 1.6%
VII	724.	996	$2^-(12)2^+(2)0^+$	+.220(9)	.005(5)	-.040(11)		-

the band mixing model for E2 transitions and a second measurement would be useful.

The gamma ray spectrum was recorded in two separate measurements with accumulation times of approximately four days. The intensities of the gamma transitions are given in Table 10, where they are compared with the results of reference 1.

C. ^{232}U

Previous studies[5] of ^{232}U revealed close lying beta and gamma bands, with reduced transition strength for E2 decay of the gamma band to the beta band 16 times that for decay to the ground state band. Because of the large errors in the measured intensities, it was not possible to make a definitive test of the single parameter band mixing model for transitions from the gamma band. We have investigated the decay of ^{232}Pa to ^{232}U with errors in the relative intensities of a few per cent using solid state detectors with these results in mind.

1. Gamma Ray Spectrum of ^{232}Pa(1.3d)

A typical gamma ray spectrum of ^{232}Pa (1.3d) is shown in Figure 13. Three separate measurements of the spectrum were made, the period of data accumulation for each being four days. For the weaker lines, the analyzer was read out and the data analyzed several times during each run.

Table 10

Energies and Relative Intensities of the Gamma Rays in the Decay of 1200 Year ^{166*}Ho

Energies (keV)	Relative Intensities	
	This Work	Gunther and Parsignault[1]
215.6	3.81 (6)	4.15 (6)
230.5	0.29 (7)	0.32 (5)
258.9	1.41 (2)	1.42 (10)
279.6	39.0	43.6 (4)
299.3	4.79 (5)	5.45 (5)
364.9	3.21 (4)	3.72 (7)
410.5	14.9 (2)	16.8 (2)
450.7	3.87 (5)	4.30 (8)
463.9	1.59 (2)	1.66 (8)
529.1	12.6 (3)	13.0 (4)
569.6	7.3 (2)	7.08 (14)
593.4	0.76 (3)	0.74 (10)
610.2	1.96 (8)	1.59 (32)
644.4	0.18 (2)	0.31 (3)
669.5	7.15 (19)	7.35 (29)
690.3	1.75 (4)	1.62 (8)
710.6	72.0 (15)	71.5 (7)
751.5	16.0 (3)	15.2 (3)
777.9	3.99 (8)	3.88 (6)
809.5	75.9 (15)	76.4 (8)
829.7	12.8 (4)	12.9 (3)
874.7	0.93 (3)	0.91 (4)
950.0	3.56 (8)	3.16 (12)
1010.5	0.11 (2)	0.11 (3)
1282.2	0.24 (2)	0.22 (2)

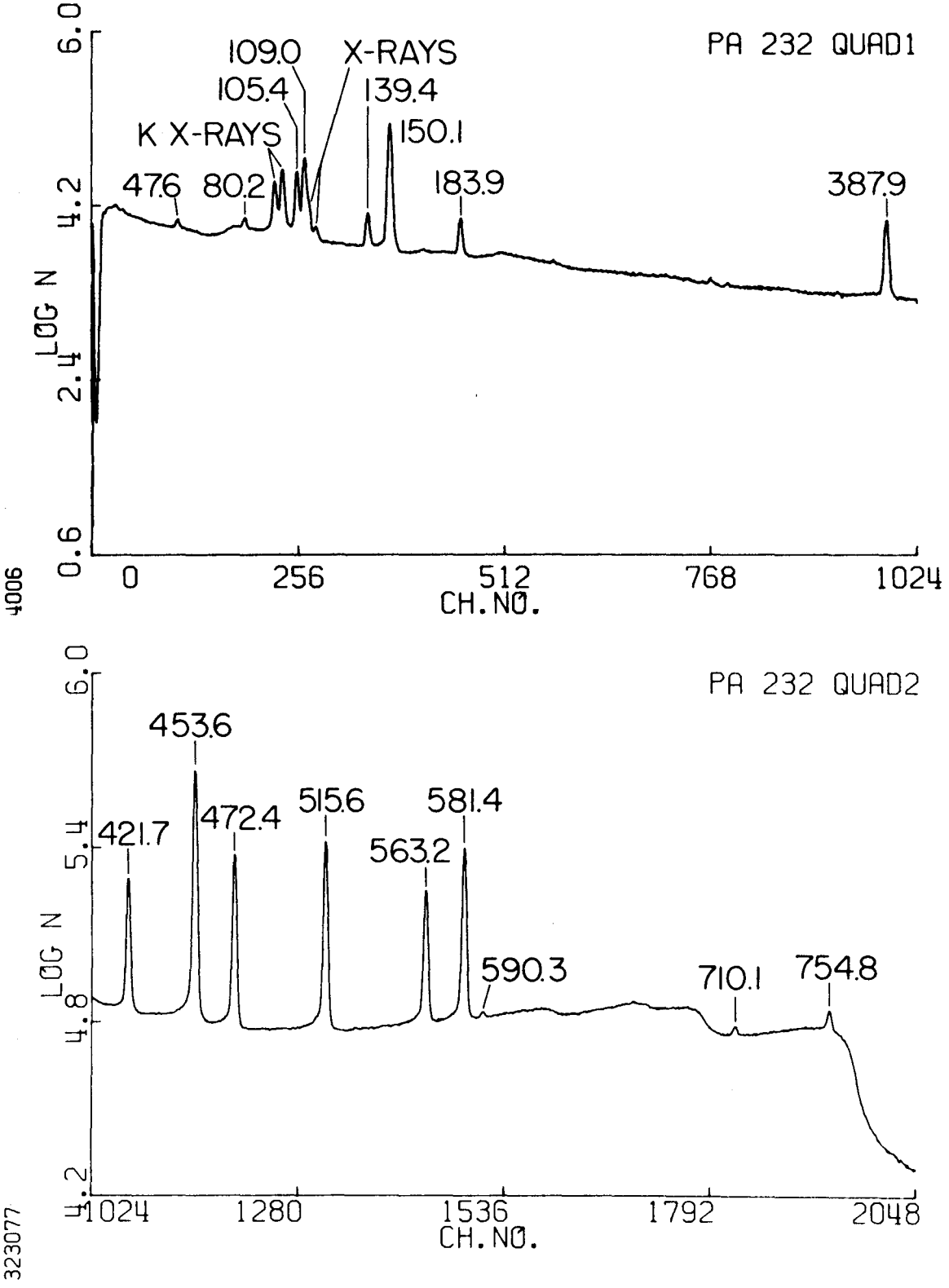

Figure 13a

The gamma ray spectrum of ^{232}Pa.

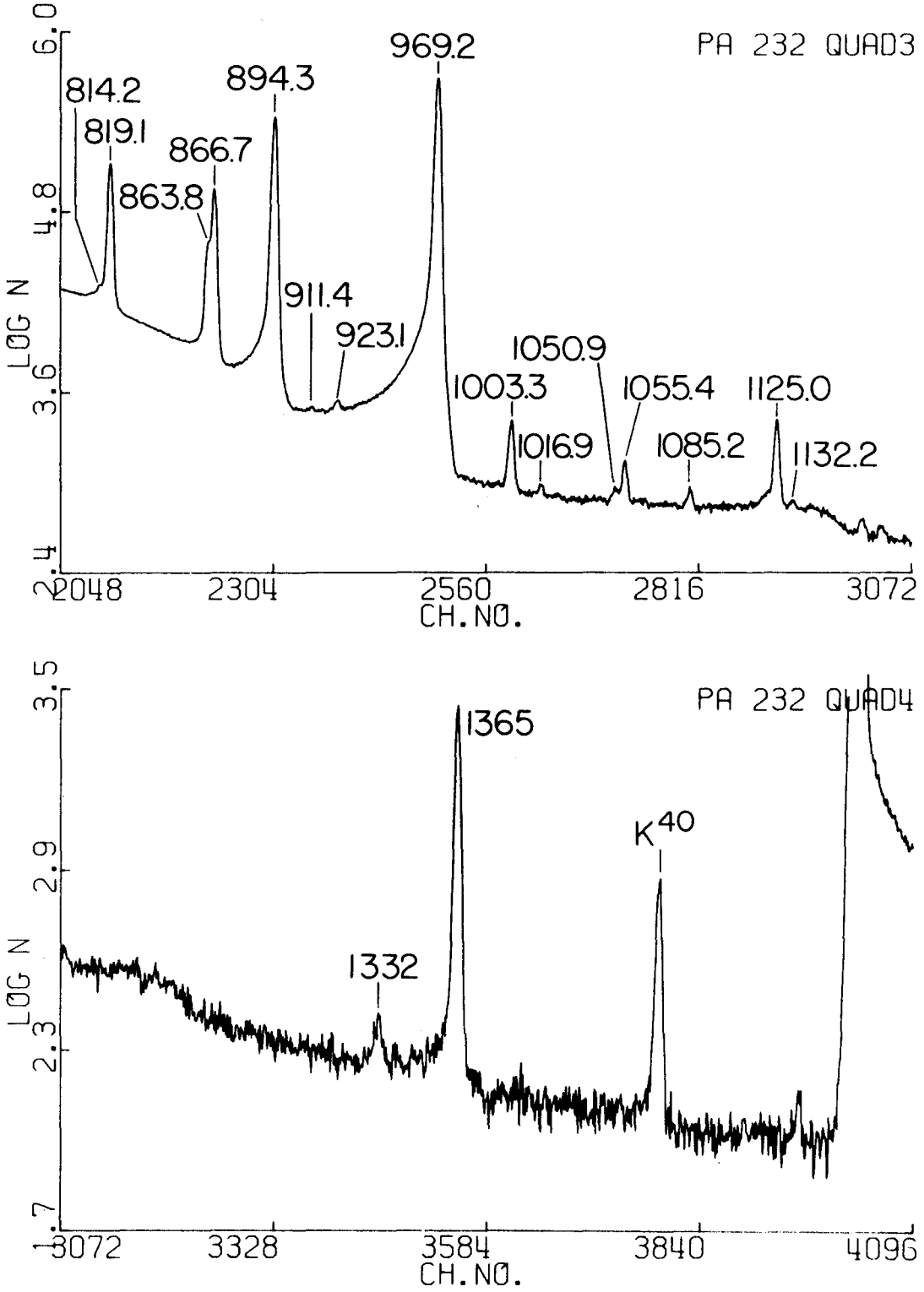
PA 232 QUAD3
969.2
894.3
814.2
819.1
866.7
863.8
911.4
923.1
1050.9
1003.3
1055.4
1125.0
1016.9
1085.2
1132.2
LOG N
6.0
4.8
3.6
2.4
2048
2304
2560
2816
3072
CH. NO.
PA 232 QUAD4
1365
K40
1332
LOG N
3.5
2.9
2.3
1.7
3072
3328
3584
3840
4096
CH. NO.

Figure 13b

The low energy gamma to beta band transitions were also measured in coincidence with the 150.1 keV line, using a fast-slow system with time resolution of 20 ns. The 150.1 keV line was taken in a 7.6x7.6 cm NaI detector, with the gamma ray spectrum in coincidence in the Ge(Li) detector recorded in the multi-channel analyzer.

The low energy gamma ray spectrum of ^{232}Pa was also studied with the 2 meter bent crystal spectrometer. These studies revealed that the 139.2 keV line observed in the Ge(Li) spectrum was actually two lines, one with a half-life longer than 1.3 days. This was taken into account in the intensity reported for this line. The line reported at 81.2 keV was also found to have a longer half-life than 1.3 days. This line was previously placed as the 3^+-4^+ transition, but our energy values give this energy as 78.3 keV. We did not observe a line of this energy. The 80.0 keV line originates in the decay of the 1050.8 keV level.

The energies and relative intensities derived from these measurements are given in Table 11, where the results are compared with those of Bjornholm,[5] et al.

2. Conversion Electron Spectrum of ^{232}Pa(1.3d)

The electron spectrum following the decay of ^{232}Pa was recorded in the electron spectrometer described above. The

Table 11

Energies and Relative Intensities of Gamma Rays and EO Conversion Electrons in the Decay of ^{232}Pa

Energy	Relative Intensities This Work	Bjornholm[5]
47.6	*	
78.3+		
80.0	*	0.13
81.2+		0.02
105.4	1.54 (5)	2.1
109.0	2.63 (6)	3.0
132.2	0.010 (5)	0.02
139.2+	0.57 (5)	0.7
150.1	11.0 (5)	12
165.0	0.030 (5)	
175.4	0.010 (2)	0.025
176.8	0.004 (2)	0.020
183.9	0.98 (6)	1.65
219	0.005	
282.2	0.010 (5)	
387.9	6.91 (15)	7.2
421.7	2.44 (7)	2.5
453.6	8.78 (24)	5.0
472.4	4.27 (11)	4.1
515.6	5.72 (14)	3.3
563.2	3.96 (9)	2.3
581.4	6.52 (15)	6.2
590.3	0.101 (15)	
645.	0.02	0.033
676.5(EO)	0.009 (1)	0.016
687.0(EO)	0.042 (2)	0.056
691.3(EO)	0.021 (1)	0.029
710.1	0.22 (1)	0.23
754.8	0.56 (3)	0.67
814.2	0.10 (3)	
819.1	7.74 (8)	8.2
863.8	1.99 (7)	2.8

Energy	Relative Intensities This Work	Bjornholm[5]
866.7	5.95 (15)	6.3
894.3	20.7 (3)	21
911.4+	0.012 (1)	
923.1	0.045 (3)	
969.2	44.6 (5)	41
1003.3	0.163 (8)	
1016.9	0.013 (2)	
1050.9	0.018 (2)	
1055.4	0.070 (4)	
1085.2	0.026 (2)	
1125.0	0.223 (10)	
1132.2	0.008 (3)	
1162		
1171		
1193		

*Intensity not measured

+See text

Table 12

Electron Intensities in the Decay of ^{232}Pa

Gamma Ray Energy (keV)	K Electron Intensity	Experimental α_k	Theoretical α_k	Admixture
387.9	0.47	6.0 (-2)	E2 4.69(-2)	4% M1
421.7	0.28	9.8 (-2)	E2 4.01(-2)	20% M1
453.6	0.60	5.8 (-2)	E2 3.50(-2)	10% M1
581.4	0.051	7.2 (-3)	E1 8.17(-3)	
676.5(E0)	0.008	-		
687.0(E0)	0.040	-		
691.3(E0)	0.020	-		
710.1	*	1.7 (-2)	E2 1.55(-2)	
754.8	*	1.6 (-2)	E2 1.39(-2)	
819.1	0.094	1.27 (-2)	E2 1.21(-2)	
863.8	*	1.56 (-2)	E2 1.10(-2)	
866.7	*	1.16 (-2)	E2 1.09(-2)	
894.3	0.073	3.77 (-3)	E1 3.73(-3)	
969.2	0.134	3.12 (-3)	E1 3.24(-3)	

*Values for electron intensities not measured are from Reference 5.

spectrum is shown in Figure 14. The accumulation time was two days. The energies, intensities, and multipolarities are given in Table 12.

3. Level Structure of ^{232}U

The gamma ray and conversion electron measurements can be summarized in the decay scheme shown in Figure 15. The quantity $h^2/2\mathcal{I}$ for each band is given in Table 13.

Table 13

Band	$\hbar^2/2\mathcal{I}$
Ground State	7.94
Octupole (0^-)	6.58
Beta (0^+)	7.21
Gamma (2^+)	7.45
(2^-)	5.67
(1^-)	6.56

a. Ground State Band.

The 0^+, 2^+, and 4^+ members of the ground state rotational band occur at 0, 47.6, and 156.6 keV. The 6^+ level is placed at 321.6 keV on the basis of the 165.0 keV line observed in the gamma spectrum and the prediction of the rotational energy formula.

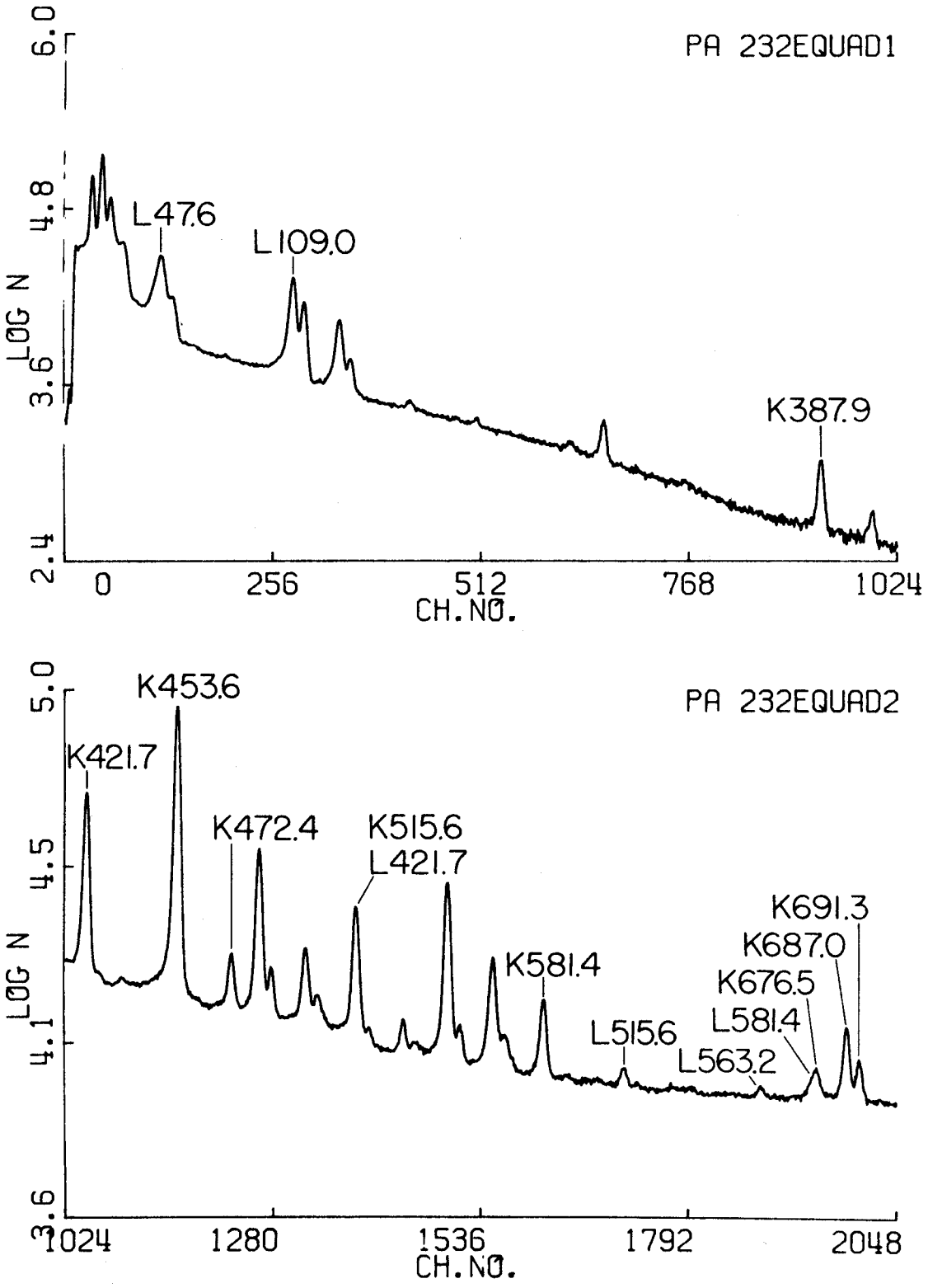

Figure 14a

The electron spectrum of ^{232}Pa.

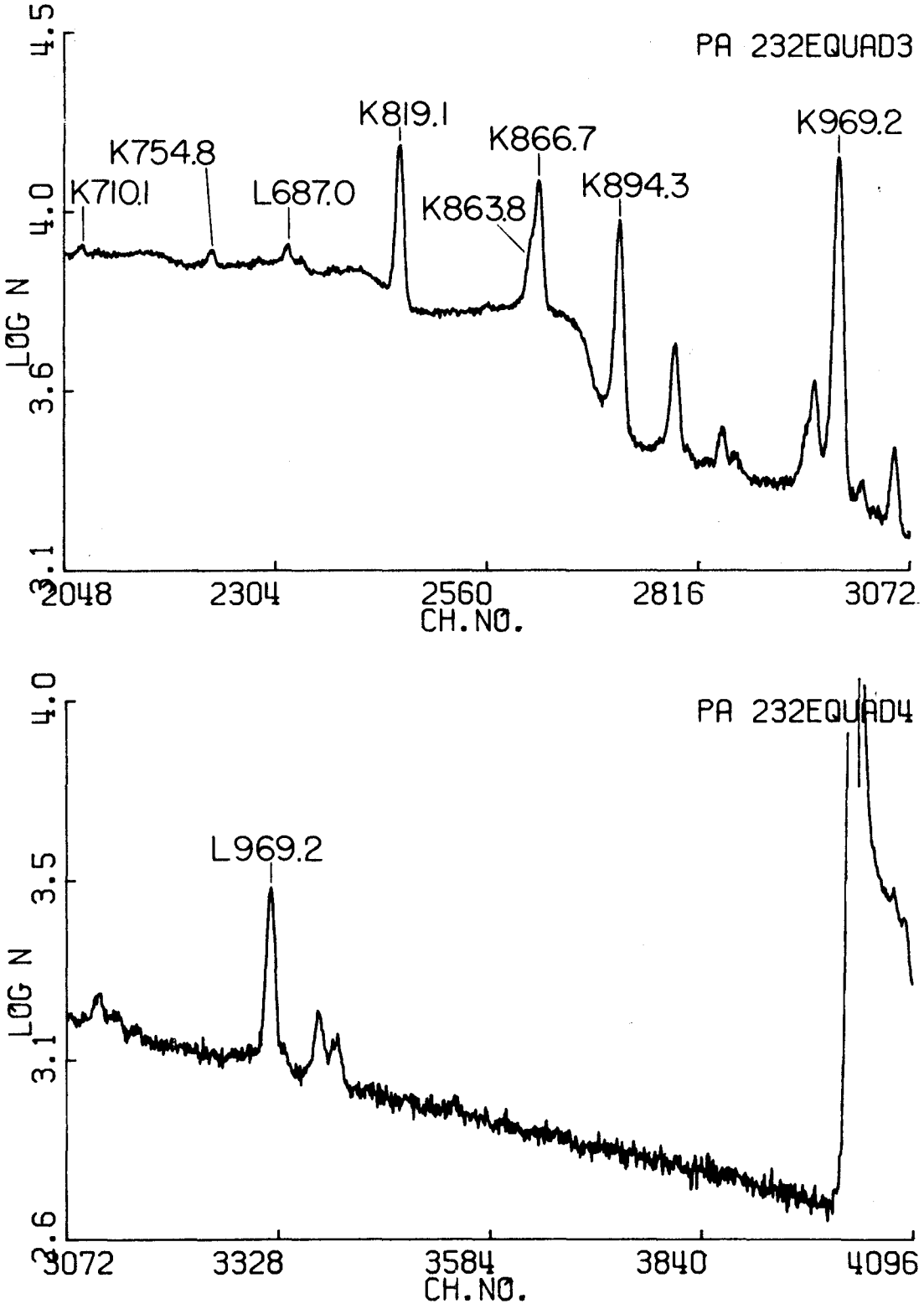
PA 232EQUAD3
K710.1
K754.8
L687.0
K819.1
K863.8
K866.7
K894.3
K969.2
LOG N
4.5
4.0
3.6
3.1
2048
2304
2560
2816
3072
CH. NO.
PA 232EQUAD4
L969.2
LOG N
4.0
3.5
3.1
2.6
3072
3328
3584
3840
4096
CH. NO.

Figure 14b

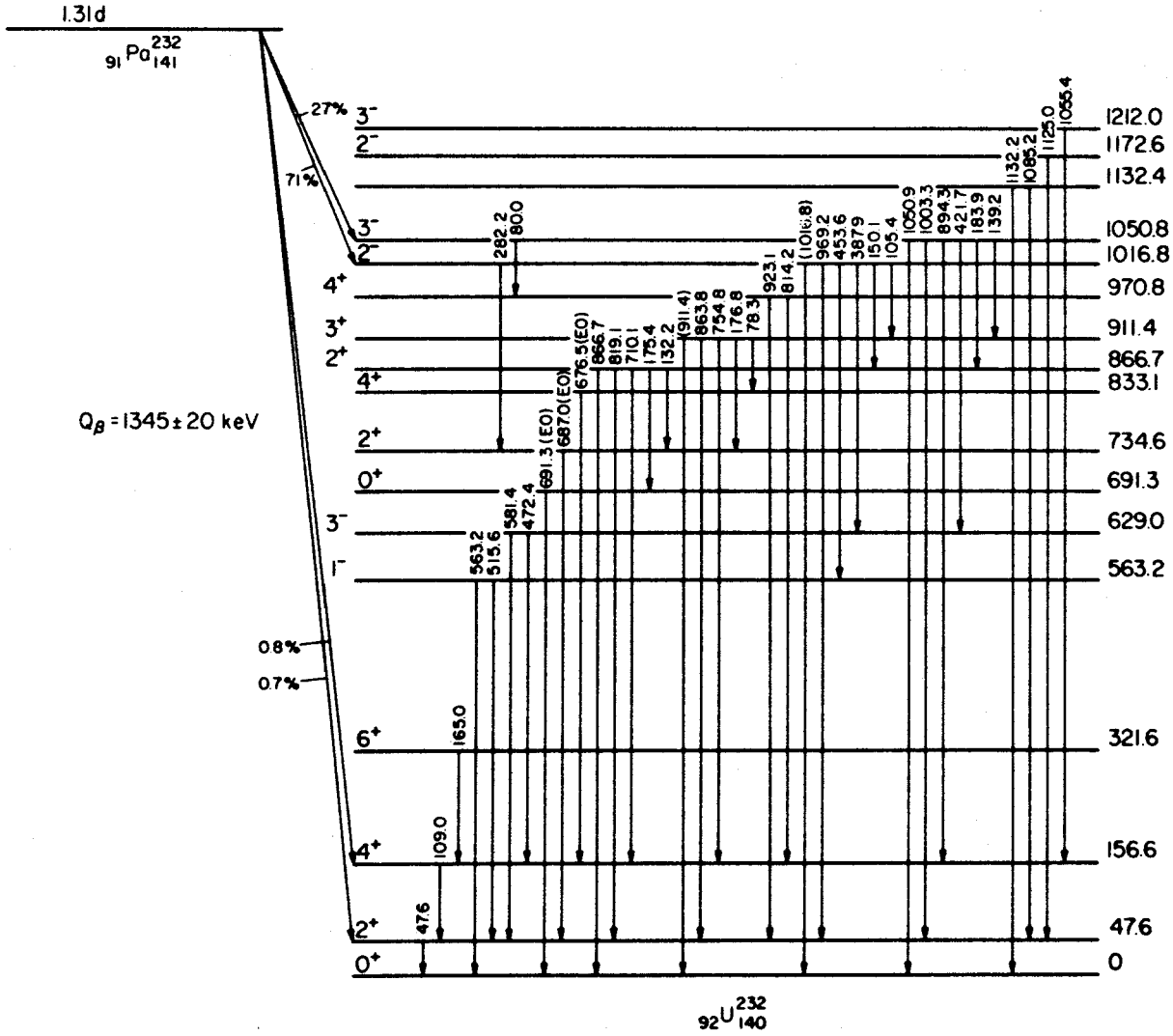

Figure 15

The decay scheme of ^{232}U.

b. Beta Vibrational Band.

The 0^+, 2^+, 4^+ members of the beta band are placed at 691.3, 734.6, and 833.1 keV. These energies are based on the EO transitions observed in the conversion electron spectrum. The placing of the levels follows the interpretation of Bjornholm, et al.[5]

c. Gamma Vibrational Band.

The 2^+, 3^+, and 4^+ members of the gamma band are placed at 866.7, 911.4, and 970.8 keV, respectively.

d. $K=0^-$ Octupole Band.

Levels with spin 1^- and 3^- are located at 563.2 and 629.0 keV. The transitions to the ground state band are E1 as shown by the internal conversion results. The reduced branching ratios show excellent agreement with predictions of the rotational model. These ratios are given in Table 14.

e. $K^{\pi}=2^-$ Band.

The levels at 1016.8 and 1050.8 are the 2^- and 3^- members of a proposed K=2 band. The K assignment is based on the reduced gamma ray branching ratios given in Table 14. The B(E1) ratios agree with K=2, and not with K=1. Also, the B(E1) strength of the 969.2 keV line is retarded 65 times with respect to the 150.1 keV transition, which can be understood if K=2, since the E1 transition would be K forbidden. The reduced

Table 14

Octupole Band to Ground-State Band

Transition	Energy	Relative B(E2)	Theory $K_i = 0$	Theory $K_i = 1$
$1^- - 0^+$	563.2	1.00	1.00	1.00
$1^- - 2^+$	515.6	1.88 (8)	2.00	0.50
$3^- - 2^+$	581.4	1.00	1.00	1.00
$3^- - 4^+$	472.4	1.22 (4)	1.33	0.75

Proposed $K^\pi = 2^-$ Band

Transition	Energy	Relative B(E1)	Theory $K_i = 2$	Theory $K_i = 1$
$2^- - 2^+_\beta$	150.1	2.46	2.00	1.00
$2^- - 3^+_\beta$	105.4	1.00	1.00	2.00
$2^- - 2^+_{G.S.}$	969.2	0.037		
$3^- - 2^+_\beta$	183.9	0.75	0.72	0.12
$3^- - 3^+_\beta$	139.2	1.00	1.00	1.00
$3^- - 4^+_\beta$	80.		1.29	1.29
$3^- - 2^+_{G.S.}$	1003.5	0.005	1.	1.33
$3^- - 4^+_{G.S.}$	894.3	1.00	2.3	1.00

	To $K^\pi = 0^-$ Octupole		Relative B(E2)	$K_i = 2$	$K_i = 1$
$2^- - 1^-$	453.6	5% M1	0.34	4.0	0.25
$2^- - 3^-$	387.9	10% M1	1.00	1.0	1.0

branching ratio for the transitions from the 3^- level at 1050.8 keV to the ground state band does not agree with K=1. An expression for K forbidden transitions is given in reference 18.

$$B(L, I_i \rightarrow I_f) \sim \langle I_i\ L\ (K_i - \nu)\ (K_f - K_i + \nu)\ |I_f\ K_f\rangle^2$$

$$K = |K_i - K_f| \quad , \quad \nu = \Delta K - L$$

The predicted ratio is 1.33, the same as for K=1, and does not give agreement.

The multipolarity of transitions from the $K=2^-$ band to the $K=0^-$ band are E2 with small M1 admixtures as determined from the internal conversion results given in Table 12 . Absolute K conversion coefficients were obtained using a normalization of known pure transitions. The 472.4, 894.3, and 969.2 keV lines were considered pure E1, the 819.2 keV line pure E2, and tables of internal conversion coefficients then were used to calculate the pure coefficients for all other lines. The possibility of large mixing in the $K=2^-$ band is evident in the reduced branching ratios from the 2^- level given in Table 14.

f. <u>K=1$^-$ Band</u>.

A $K=1^-$ band is proposed with 2^- and 3^- levels at 1172.6 and 1212.0 keV.[47] The spins are based on decay to the ground state band. The level at 1132.4 appears to be 1^- from branching to the ground state band. However, the 1^- level of the band should

be at 1145 keV, based on the energy spacing derived from the 2^- and 3^- levels.

g. Mixing of the Negative Parity Levels.

A possible explanation of the lack of agreement of experimental and predicted reduced branching ratios for transitions from the 2^- to to 0^- band is mixing of the bands through the operator

$$h_{2+} I_-^2 + h_{2-} I_+^2$$

This leads to the expression for B(E2) given by Michailov[48]

$$B(E2) = 2 \langle I_1 22-2 | I_2 0 \rangle^2 \left\{ M_1 + M_2 [I_2(I_2+1) - I_1 (I_1+1)] \right\}^2$$

The experimental ratio M_2/M_1 is 0.13, corresponding to a z parameter of 0.54. This is very large compared to the parameter z_2 for the gamma band of 0.025. Similar results are seen in ^{234}U [49] where levels through 7^- have been observed. If the interband B(E2) is assumed to be one single particle unit, and the intraband B(E2) equal to the ground state band value of 200 spu, the reduced mixing amplitude is $\epsilon_2 = 0.007$. This value of the mixing parameter ϵ_2 is too large to account for the observed energy shifts. This is in contrast to mixing of the gamma band, where the mixing parameter leads to a contribution of only 10% of the observed shift.

V. ANALYSIS OF BETA AND GAMMA BAND MIXING

In this chapter, we discuss the observed B(E2) strengths for transition from the beta and gamma bands and compare these strengths with values calculated from microscopic models and from the band mixing model discussed in Chapter II.

A. ^{152}Sm and ^{154}Gd

Our experimental results for ^{152}Sm and ^{154}Gd are compared with the single parameter band mixing model in Table 15.

For ^{154}Gd, the transitions from the gamma band have been corrected for the M1 admixture. In ^{152}Sm, the 964.4 keV line has been corrected for 6% M1.[10] Transitions from the beta band are assumed pure E2, since there is no definite evidence for large M1 admixtures.[9, 10] No agreement is found with the single parameter theory in either ^{152}Sm or ^{154}Gd.

If we consider mixing of the gamma band and the beta band, the admixtures to the transition matrix element are described by two additional parameters, z_3 and z_4, respectively. In ^{152}Sm, this model gives for the branching from the 2^+ level of the beta band $z_0 = 0.044(4)$, $z_4 = 0.013(3)$, while branching from the 4^+ level gives, if $z_0 = 0.044(4)$,

Table 15. Experimental B(E2) Ratios and z-Parameter Values for ^{152}Sm and ^{154}Gd

Transition	2 0	2 2	2 4	3 2	3 4	4 2	4 4	4 6
			^{152}Sm γ-Band					
Energy	1086.0	964.4	719.4	1112.2	867.7	1249.7	1005.0	
Intensity	41.2(6)	59.1(12)	1.33(5)	55.2(7)	16.8(2)	.73(5)	2.60(13)	
Rel. B(E2)	.41	1.00	.104	.97	1.00	.099	1.00	
z_2	.091(5)		.070(8)	.080(5)		.076(9)		
			^{152}Sm β-Band					
Energy	810.7	688.7	444.1			901.2	656.5	
Intensity	1.31(4)	3.41(7)	1.28(11)			.34(17)	.62(5)	
Rel. B(E2)	.174	1.00	3.37			.07(3)	1.00	
z_0	.085(2)		.026(6)			.053 or	.090(6)	
			^{154}Gd γ-Band					
Energy	996.3	873.2	625.2	1004.8	756.9	1140.9	892.7	545.6
Intensity	10.2(2)	11.7(2)	0.32(1)	17.5(3)	4.41(5)	0.22(1)	0.49(1)	
Rel. B(E2)	.451	1.00	.144	.92	1.00	.138	1.00	
z_2	.077(5)		.123(20)	.076(4)		.060(8)		
			^{154}Gd β-Band					
Energy	815.6	692.4	444.4			924.5	676.6	346.7
Intensity	0.48(2)	1.76(4)	0.57(1)			0.06(1)	0.15(1)	
Rel. B(E2)	.119	1.00	2.94			.083	1.00	
z_0	.098(3)		.020(2)			.052 or	.091(2)	

$z_4 = 0.$ (4). In the gamma band, branching from the 2^+ state furnishes $z_2 = 0.084(6)$, $z_3 = -0.010(3)$, while for the 4^+ branching, if $z_2 = 0.084(6)$, $z_3 = +0.005(4)$ is found. In ^{154}Gd, agreement is obtained with $z_2 = 0.085(5)$, $z_3 = 0.010(3)$ for the gamma band, but again in the beta band there is apparently less mixing in the 4^+ level, the 2^+ level giving $z_0 = 0.044(4)$, $z_4 = 0.019(4)$, while the 4^+ level gives $z_0 = 0.037(6)$, $z_4 = 0.000(5)$.

Finally, the consequences of unequal quadrupole moments in the two bands can be considered.

Again, there is agreement with the gamma band of ^{154}Gd only. The values of the parameters in this case are $M_2/M_1 = 0.036$, $M_3/M_1 = 0.001$. This leads to a value for $Q_0(K=2)/Q_0(K=0) = 0.75$. Since there is no agreement for the beta band, this ratio probably has little meaning and no error is given. Meyer reports the value $Q_{22}/Q_{00} = 0.9 \pm 0.2$, which is derived from the ratio of intraband to interband transitions.

We have also observed transitions from the gamma band to the beta band. The results given in Table 16 show evidence for strong mixing of the two vibrational bands.

B. ^{166}Er

The experimental relative B(E2) strengths for transition from the gamma band are given in Table 17. There is good agreement with a value of $z_2 = 0.046(2)$.

Table 16

Transitions from the Gamma Band to the Beta Band

Transition	Energy	^{152}Sm Intensity	Rel. B(E2)	Energy	^{154}Gd Intensity	Rel. B(E2)
$2_\gamma - 0_\beta$	400.5	0.01	1.0	315.4	0.013	1
$2_\gamma - 2_\beta$	275.4	0.14	88.0	180.7	0.002	2.5
$2_\gamma - 0_\beta$	400.5	0.01	1.0	315.4	0.013	1
$2_\gamma - 0_{G.S.}$	1086.0	41.7	28.0	996.3	10.2	2.5

Table 17

z_2 Parameter for ^{166}Er

Transition γ - g. s.	Energy (keV)	B(E2) Ratio	Rotational Model	z_2
3 - 2	777.9	1.36	2.50	0.048
3 - 4	593.			
4 - 2	874.7	0.163	0.3395	0.048
4 - 4	690.3			
5 - 4	809.5	0.719	1.750	0.044
5 - 6	529.1			
6 - 4	950.0	0.086	0.269	0.043
6 - 6	669.5			
7 - 6	829.7	0.440	1.500	0.044
7 - 8	463.9			
8 - 6	1010.5	0.065	0.2395	0.034
8 - 8	644.4			

C. ^{232}U

The reduced branching ratios for transitions from the gamma band to the ground state band in ^{232}U are given in Table 18. The reduced E2 transition ratios are derived from the gamma ray measurements with the assumption that the transitions are pure E2. Small admixtures of M1, of the order of 5-10%, are not excluded by conversion electron data. A band mixing parameter $z_2 = 0.025\,(10)$ is consistent with the measured branching ratios. The reduced E2 ratios for transitions from the γ-band to the β-band are given in Table 18. These results are based on singles measurements and coincidence measurements which showed the 132.2 and 175.4 keV lines to be in coincidence with the 150.1 keV line. It is interesting to note that the relative B(E2) strength to the β-band is about 5 times that to the ground state band.

The β-band decays by EO and E2 transitions to the ground state band. Only upper limits could be estimated for the intensities of gamma lines leaving this band. The levels are based on the observed EO transitions. In a neighboring nucleus, ^{232}Th, there is also evidence for strong mixing of the beta and gamma bands.[50] Here, the 2^+ levels of the two bands are only 14 keV apart. The evidence for the mixing is the decay of the 2^+ level in the gamma band by an EO transition to the 2^+ level of

Table 18

E2 Transitions from $K^{\pi} = 2+$ Gamma Band to Beta and Ground-State Bands

Transition	Energy	Relative B(E2)	Theory	z_2
$2^+ - 0^+$	866.7	0.58 (2)	0.70	0.032 (5)
$2^+ - 2^+$	819.1	1.00	1.00	
$2^+ - 4^+$	710.1	0.058 (4)	0.05	0.015 (6)
$2^+ - 0_\beta$	175.	2.9 (6)		
$2^+ - 2_\beta$	132.	12.0 (60)		
$3^+ - 2^+$	863.8	1.81 (2)	2.50	0.026 (5)
$3^+ - 4^+$	754.8	1.00	1.00	
$4^+ - 2^+$	923.1	0.28 (9)	0.34	0.023 (20)
$4^+ - 4^+$	814.2	1.00	1.00	

the ground state band. This would be K-forbidden if there were no mixing.

There is now good experimental evidence for the correctness of these calculations in recent work on ^{234}U, [55] through stripping and pick-up experiments. The differential cross section for stripping or pick-up processes can be expressed in terms of the Nilsson wave function and the single particle transfer cross section calculated from the distorted wave Born approximation(DWBA). The cross section for population of a state I, K from an initial state I_0, K_0 is

$$\frac{d\sigma}{d\omega} = \sum_{j,l} g^2 \langle I_0\, j\, K_0\ \Delta K | IK \rangle^2\ C_{jl}^2\ \phi_l(\bullet)$$

where C_{jl} is the expansion coefficient of the Nilsson wave function $|Nn_z \Lambda\Sigma\rangle$ on the spherical function $|N_j l\, \Omega\rangle$. The $\phi_l(\bullet)$ is the intrinsic single particle transfer cross section for transfer of a neutron with angular momentum l.

Several pure single particle states are populated in ^{234}U, and these are used to normalize the excitation amplitudes. For the gamma vibrational level at 927 keV, Bjornholm finds 27% of the wave function to be $633\downarrow - 631\downarrow$, and 27% to be $743\uparrow - 761\uparrow$. Soloviev predicts 40% and 10% for these probabilities. Bes[51] finds the state more collective, i.e., many more states entering in small amounts. His results give 10% and 15% for the amplitude

squared of the states, respectively. The agreement of theory and experiment can be considered good.

In the region of transition from spherical to deformed nuclei, however, agreement with these calculations is not so good. The lack of agreement indicates that the perturbation expansion of angular momentum operators which works well for strongly deformed nuclei does not describe the nuclei in the transitional region. Recently, Kumar and Baranger[56] have made calculations to study the onset of deformation in these transitional regions. The method differs from those discussed above in the following respects: (1) no permanent deformation is assumed, and spherical shell model wave functions are used (the residual interaction is pairing plus quadrupole) (2) couplings between the rotation and vibration are treated exactly there is no linearization of the motion. The anharmonicity of the quadrupole motion in fact leads to mixing of bands in deformed nuclei and phonon mixing in spherical nuclei. Results in the transition region from tungsten to platinum show that the assumption of separation of beta and gamma vibrations is not very good. This is especially true for the W isotopes, where the bands are almost degenerate and strong mixing is found.

Preliminary calculations by Kumar[57] using a somewhat simpler model (the potential form is an analytic form rather

than the result of Hartree-Fockcalculations) have been made for transition matrix elements and shape parameters in ^{154}Sm. Most models assume the nuclear shape to be static or capable of executing small, harmonic vibrations. While this assumption may be good for spherical and strongly deformed nuclei, it is probably not good for transitional regions. Kumar makes the adiabatic approximation that the intrinsic motion follows the collective motion, but the shape is allowed to vary to fit observed parameters. These results should apply to ^{152}Sm and ^{154}Gd.

In order to obtain agreement with the observed beta and gamma band energies, a large coupling between the two bands is necessary. This coupling is caused by the mixing of states with different shapes in the excited levels. The reason for these shape fluctuations is apparent from the potential shown in Figure 16; for excitations of 2 MeV, prolate, spherical, and oblate shapes are almost equally probable. The predicted branching ratios are given in Table 19 with the results of our experiments.

The most notable successes are in the calculated values for the gamma to beta band transitions and those from the beta band to the ground state band. There is a singluar lack of agreement in fitting the gamma band to ground state band transitions; the mixing predicted by Kumar is too small to account for the experimental data.

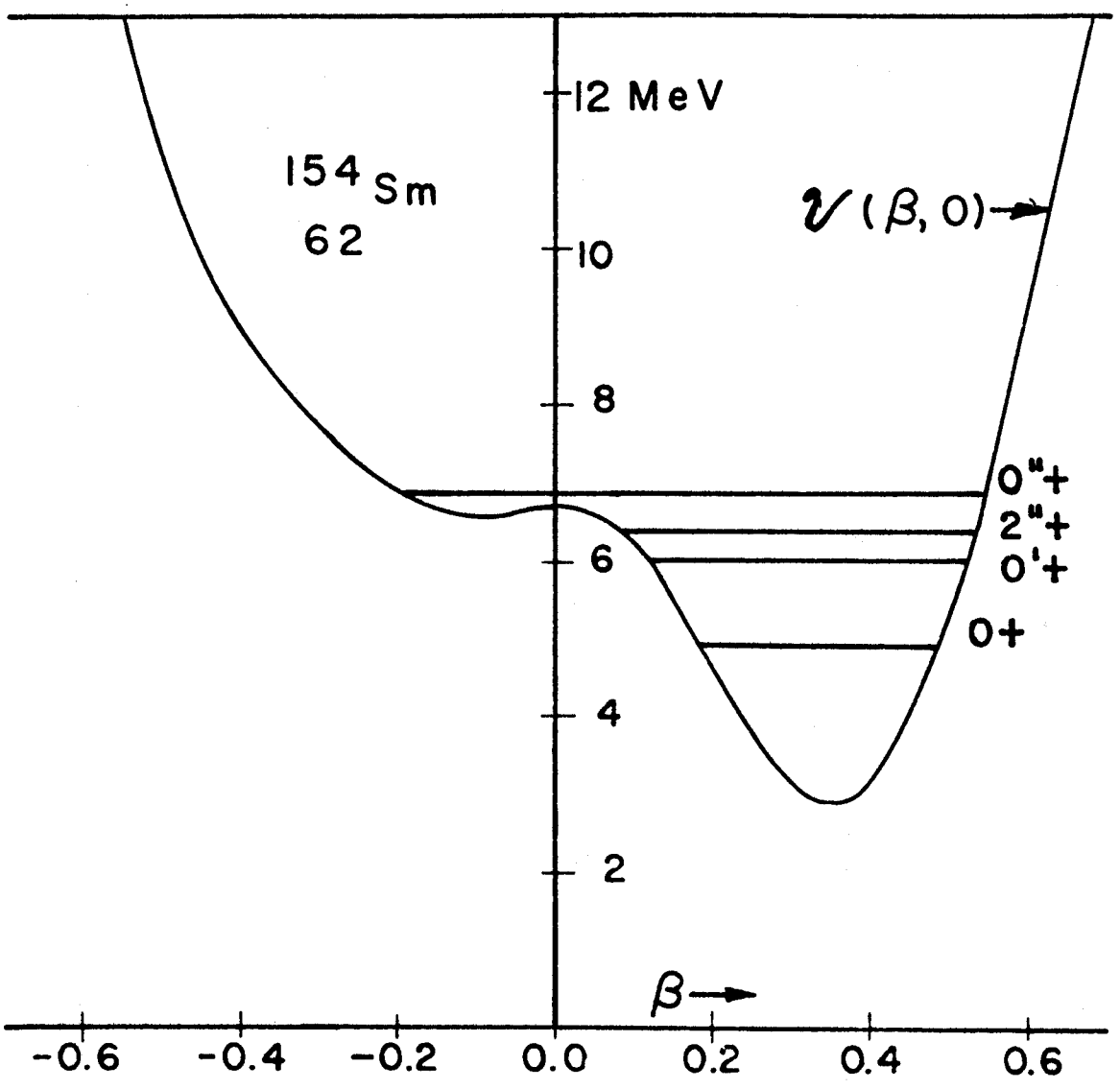

Figure 16

Band-heads in the potential well of ^{154}Sm. Beta is negative for oblate, positive for prolate deformation. Taken from reference 57.

Table 19

Comparison of Experimental B(E2) Ratios with Calculations of Kumar [57]

Transition	Predicted B(E2) Ratio		Observed B(E2) Ratio	
	Kumar	Rotational	^{152}Sm	^{154}Gd
$2_\gamma \rightarrow 2_\beta$ $2_\gamma \rightarrow 2_{G.S.}$	1.57	-	3.	1.
$2_\gamma \rightarrow 0_\beta$ $2_\gamma \rightarrow 2_\beta$	0.054	0.70	0.01	0.40
$2_\beta \rightarrow 0_{G.S.}$ $2_\beta \rightarrow 2_{G.S.}$	0.25	0.70	0.17	0.12
$4_\beta \rightarrow 2_{G.S.}$ $4_\beta \rightarrow 4_{G.S.}$	0.21	1.1	0.07	0.08
$2_\gamma \rightarrow 0_{G.S.}$ $2_\gamma \rightarrow 2_{G.S.}$	0.72	0.70	0.41	0.45
$4_\gamma \rightarrow 2_{G.S.}$ $4_\gamma \rightarrow 4_{G.S.}$	0.32	0.34	0.10	0.14

In addition to these results, several calculations have been made using a single particle states of a deformed shell model. The amplitudes of the states are calculated according to a model developed by Nilsson[54], with the resulting single particle levels identified by their asymptotic quantum numbers. A brief discussion of the Nilsson model is given in Appendix B. From these single particle states, the parameters of which are determined from odd-A nuclei, states in neighboring even-even nuclei can be formed. These excited states are of two types; two quasi-particle states (states made up of two single particle states with the pairing interaction included), and collective states made up of a coherent combination of two quasi-particle states. These states will have K as a good quantum number. Residual interactions are then included which mix in states with different K values.

Pavlichenkov[52] has calculated the value of z_2 using the rotation-vibration interaction in the form

$$h_{\pm 2} = -\frac{\Gamma_2}{4\mathcal{J}_0} A^{\dagger}_{\mp 2}$$

where $\mathcal{J}_0$ is the moment of inertia and $A^{\dagger}_{\mp 2}$ is the phonon production operator. The parameter Γ_2 is a function of three experimentally determined quantities; equilibrium deformation β, pairing energy Δ, and gamma vibrational energy $\hbar\omega_\gamma$.

Bes[51] has used the Coriolis interaction to calculate the mixing through intermediate K=1 states. Pairing and quadrupole forces are included, and the amplitudes of all K=1 states contributing to the collective gamma band are found. M1 transitions are allowed through the K=1 states, and multipole mixing ratios are given. Deformation and pairing energy are taken from experiment; the strength of the quadrupole interaction is the only free parameter. Marshalek[17] has also made detailed calculations of phenomenological parameters using the Coriolis interaction.

Bes[51] and Soloviev[53] have calculated the energy and composition of excited states in deformed nuclei. These results were discussed above with regard to ^{232}U.

A comparison of the values obtained in these separate calculations for the z parameter and the experimental values can be made using the results in Table 20. The results for the strongly deformed nuclei agree reasonably with the calculations.

Table 20

Comparison of Experiment and Microscopic Calculations of z_o and z_2

Isotope	z_2				
	Pavlichenkov[52]	Bes[51]	Marshalek[17]		Experiment
^{152}Sm	0.064	0.035	0.089	0.046	*
^{154}Gd	0.079	0.060	0.099	0.055	*
^{166}Er	0.028	0.022	0.076	0.033	0.046(2)
^{232}U	-	0.024	0.039	0.074	0.025(10)
		z_o			
^{152}Sm			0.062		*
^{154}Gd			0.063		*
^{232}U			0.023		

*No single z fits all B(E2) ratios.

VI. CONCLUSIONS

We have described experimental techniques for precision measurement of energies, intensities, and multipolarities of gamma rays and electrons following radioactive decay. Using these techniques, we have studied several even-even deformed nuclei. Several additions were made to existing decay schemes, and particular attention was paid to transitions from the beta and gamma vibrational bands. Good agreement is found with the unified collective model, including first order band mixing, for the gamma band of the strongly deformed nuclei ^{166}Er and ^{232}U. No agreement is found for the transition nuclei ^{152}Sm and ^{154}Gd. The possibility that the lack of agreement may be due to M1 admixtures in the transitions may be discounted from the results of recent Coulomb excitation experiments. Some degree of success in explaining the B(E2) ratios has been attained by Kumar and Baranger, using a model which allows for mixing of different shape modes in the excited states. The results are not in good quantitative agreement at present, but these calculations appear to have validity for the transition nuclei. More careful measurements of gamma to beta band transitions would be useful, and further information can be gained

by Coulomb excitation experiments, since these are very sensitive to the matrix elements connecting the beta and gamma bands. Stripping and pick-up reactions give information on the composition of the collective states.

Apart from the low lying octupole bands, there is poor agreement with the rotational model values for reduced branching ratios for the negative parity bands in the nuclei studied. First order band mixing is not able to account for the experimental results. These states are at high energy, and there may be mixing with a large number of states.

APPENDIX A

Rotational Wave Functions and Energy Levels

The rigid body Hamiltonian T_{rot} can be written:

$$T_{Rot} = \frac{\hbar^2}{2\mathcal{I}_{x'}} R_{x'}^2 + \frac{\hbar^2}{2\mathcal{I}_{y'}} R_{y'}^2 + \frac{\hbar^2}{2\mathcal{I}_{z'}} R_{z'}^2$$

where R_i is the rotation operator about the i axis. In practice, the $\mathcal{I}$'s are treated as empirical constants. The value is larger than that predicted for irrotational flow, but less than the moment for a rigid rotor. If the body has axial symmetry about the Z' axis, $\mathcal{I}_{x'} = \mathcal{I}_{y'} = \mathcal{I}$, and using the relation $\bar{R} = \bar{I} - \bar{J}$, the kinetic energy of rotation becomes:

$$T_{Rot} = \frac{\hbar^2}{2\mathcal{I}} \left[\vec{I}^2 + \vec{J}^2 - 2(\vec{I}\cdot\vec{J}) \right] + \left(\frac{\hbar^2}{2\mathcal{I}_{z'}} - \frac{\hbar^2}{2\mathcal{I}} \right) \left[\vec{I}_{z'} - \vec{J}_{z'} \right]^2$$

In looking for appropriate eigenfunctions, we note that $D^I_{MK}(\vartheta)$ is an eigenfunction of the following operators:

$$I^2 D^I_{MK}(\vartheta) = \hbar^2 I(I+1) D^I_{MK}(\vartheta)$$

$$I_z D^I_{MK}(\vartheta) = \hbar M D^I_{MK}(\vartheta)$$

$$I_{z'} D^I_{MK}(\vartheta) = \hbar K D^I_{MK}(\vartheta)$$

The quantum numbers are shown in Figure 1.

The product wave function

$$\Psi \sim D^I_{MK}(\vartheta)\, \chi_\Omega(x')$$

is an eigenfunction of H_{intr} and T_{rot} with the exception of

two terms

$$-\frac{\hbar^2}{2\mathcal{J}}(\vec{I}\cdot\vec{J}) \quad , \quad \frac{\hbar^2}{2\mathcal{J}}\vec{J}^2$$

Since H_{intr} has not been defined, the $\vec{J}^2$ term can be incorporated in H_{intr}. The $\vec{I}\cdot\vec{J}$ term is the Coriolis energy and mixes states with K differing by one unit.

Symmetry tests require,[1] for $K\neq 0$,

$$\psi(IKM) = \left[\frac{2I+1}{16\pi^2}\right]^{1/2} A\left\{D^I_{MK}(\vartheta)\,\chi_K(x') + B\,D^I_{M-K}(\vartheta)\,\chi_{-K}(x')\right\}$$

$$A = \begin{matrix} 1 & \pi = + \\ i & \pi = - \end{matrix} \qquad B = \begin{matrix} (-)^{I+K} & \pi = + \\ -(-)^{I+K} & \pi = - \end{matrix} \qquad \pi = \text{PARITY}$$

For K=0, which includes the ground state band of even-even, axially symmetric deformed nuclei,

$$\psi(IOM) = \left[\frac{2I+1}{8\pi^2}\right]^{1/2} A\,D^I_{MO}(\vartheta)\,\chi_0(x')$$

$$A = \begin{matrix} 1 & \pi = + \\ i & \pi = - \end{matrix}$$

The values of I allowed are

$$K^\pi = 0^+ \qquad I^\pi = 0^+, 2^+, 4^+ \cdots$$
$$K^\pi = 0^- \qquad I^\pi = 1^-, 3^-, 5^-$$

The energy levels are found by considering the Hamiltonian in the form

$$H_{INTR} + \frac{\hbar^2}{2\mathcal{J}}\vec{I}^2 + H_{COUPL}$$

H_{coupl} is small, and H_{intr} contributes the same to each member of the band, so the energy levels for a given band are given by

$$\frac{\hbar^2}{2\mathcal{J}}\vec{I}^2\,\psi(IKM) = \frac{\hbar^2}{2\mathcal{J}}I(I+1)\,\psi(IKM)$$

When we speak of a collective vibrational state, it is implied that the state is a coherent superposition of many

excitations (two quasi-particle states), each entering with a small aplitude. For the rare earths, the amplitudes calculated by Bes[51] for the gamma band appear to confirm this interpretation. However, it is not excluded that the observed levels could be produced by a small number of excitations interacting through residual forces. Transition strengths between bands are only a few single particle units compared to approximately 100 for the collective intraband transitions.

Octupole vibrations are also possible. The value of the phonon angular momentum is 3, with projection on the symmetry axis ν^{π} =0⁻, 1⁻, 2⁻, 3⁻. The 0⁻ band appears most frequently, often below 1 MeV, and is calculated to be the most collective. ^{232}U is an example in which bands with K =0⁻, 1⁻, 2⁻ have been identified.

Transition Probabilities

The transition rate T for the decay of a nuclear level by gamma radiation of energy E and multipole λ is given (in the long wave length limit) by the relation

$$T = \frac{8\pi(\lambda+1)}{\lambda[(2\lambda+1)!!]} \frac{1}{\hbar}\left(\frac{E}{\hbar c}\right)^{2\lambda+1} B(\lambda, I_i \rightarrow I_f)$$

$$B(\lambda, I_i \rightarrow I_f) = \frac{1}{2I_i+1} \sum_{m_i} \sum_{m_f} \langle I_f m_f | \mathcal{M}(\lambda) | I_i m_i \rangle^2$$

In the case of E2 radiation, the operator M (λ) is given by

$$Q_q^{(2)} = \sqrt{\frac{16\pi}{5}} \sum_p r^2(p)\, Y_q^{(2)}(\phi_p, \theta_p)$$

where the sum is overall protons in the nucleus. The operator can be referred to the intrinsic coordinate frame by use of the rotation operator:

$$Y_q^{(2)} = \sum_{q'} D_{qq'}^{(2)}(\vartheta) \left\{ Y_{q'}^{(2)} \right\}_{\vartheta}$$

, where $\{\}_{\vartheta}$ indicates the intrinsic system.

The matrix element can be calculated using the product wave function $|I_i K_i\rangle = \left[\frac{2I_i+1}{8\pi^2}\right]^{1/2} D_{MK_i}^{I_i}\, \chi_{K_i}$

Performing the integration over angular coordinates,

$$\langle I_f M_f | \mathcal{M}(E2) | I_i M_i \rangle = \left[\frac{2I_f+1}{2I_i+1}\right]^{1/2} \times$$

$$\times \sum_{q'} (I_i 2\, M_i\, q | I_f M_f)(I_i 2\, K_i\, q' | I_f K_f)\left(\chi_f \left| \sqrt{\tfrac{16\pi}{5}} \sum_p r^2(p) \{Y_{q'}^{(2)}\}_{\vartheta} \right| \chi_i\right)$$

The intrinsic matrix element is the same for all members of the band

$$Q_{K_i K_f} = \left(\chi_{K_f} \left| \sqrt{\tfrac{16\pi}{5}} \sum_p r^2(p) \{Y_{q'}^{(2)}\}_{\vartheta} \right| \chi_{K_i}\right)$$

The angular momentum dependence is contained in the Clebsch-Gordan coefficient. Summing over magnetic substates, the B(E2) value becomes:

$$B(E2) = \frac{1}{2I_i+1} \langle I_i 2\, K_i\, (K_f - K_i) | I_f K_f \rangle^2 Q_{K_i K_f}^2$$

For transition from an initial level I_i K_i to final levels I_f and I_f', K_f, the intrinsic matrix element divides out and

$$B(E2) \sim \langle I_i 2 K_i (K_f - K_i) | I_f K_f \rangle^2$$

Vibrations

Spherical Nuclei

The energy levels below 2-3 MeV of spherical nuclei can be understood by considering these modes as collective vibrations of the nucleus. The shape of the surface can be[15] expanded in spherical harmonics

$$R(\theta,\phi) = R_0 \{ 1 + \sum_{\lambda\mu} \alpha_{\lambda\mu} Y_\mu^{(\lambda)} (\theta,\phi) \}$$

The $\alpha_{\lambda\mu}$ can be used as dynamical variables. The Hamiltonian can be written

$$H_c = \sum_{\lambda\mu} \{ \tfrac{1}{2} B_\lambda |\dot{\alpha}_{\lambda\mu}|^2 + \tfrac{1}{2} C_\lambda |\alpha_{\lambda\mu}|^2 \}$$

The solutions are those of a harmonic oscillator, and the excitations can be regarded as phonons. ^{152}Gd shows a typical level scheme, Figure 10. The first excited state is 2^+, a one phonon state, with enhanced B(E2) strength to the ground state. The triplet states 0^+, 2^+, 4^+ are interpreted as two phonon excitations. Transitions from these states to the one phonon state are enhanced; those to the ground state are retarded, as shown in Table 7. In this model all M1 transitions are retarded.

Spheroidal Nuclei

For quadrupole vibrations, the nuclear surface can be

described in terms of 5 parameters

$$R(\theta,\phi) = R_0\left\{1 + \sum_{\mu=-2}^{2} \alpha_\mu Y_\mu^{(2)}(\theta,\phi)\right\}$$

The $Y_\mu^{(2)}$ can be referred to a coordinate system fixed in the nucleus, and the five parameters become the three Euler angles specifying the orientation of the ellipsoid and two parameters describing the shape, β and γ. The three axes of the ellipsoid become

$$R_i(\theta,\phi) = R_0\left\{1 + \sqrt{\frac{5}{4\pi}}\,\beta\,\cos\left(\gamma - \frac{2\pi i}{3}\right)\right\} \qquad i=1,2,3$$

The parameter γ determines the shape, which is axially symmetric only for certain values of γ.

$\gamma = 0$ PROLATE SPHEROID

$\gamma = \pi$ OBLATE

$\gamma = \pi/3$ or $2\pi/3$ AXIALLY SYMMETRIC (x' or Y')

The phonon angular momentum is not a good quantum number, but the projection on the symmetry axis is. For beta vibrations, $\nu = 0$, for gamma vibrations, $\nu = 2$. Figure A. 1 shows schematically the vibrations. A typical spectrum of a deformed nucleus is given in Figure 12.

Transitions from the β and γ bands to the ground state band are collective, but less so than transitions within a rotational band. Measured values are given in Table A1. For the gamma band, $\Delta K = 2$ and the transitions are predominantly E2. The

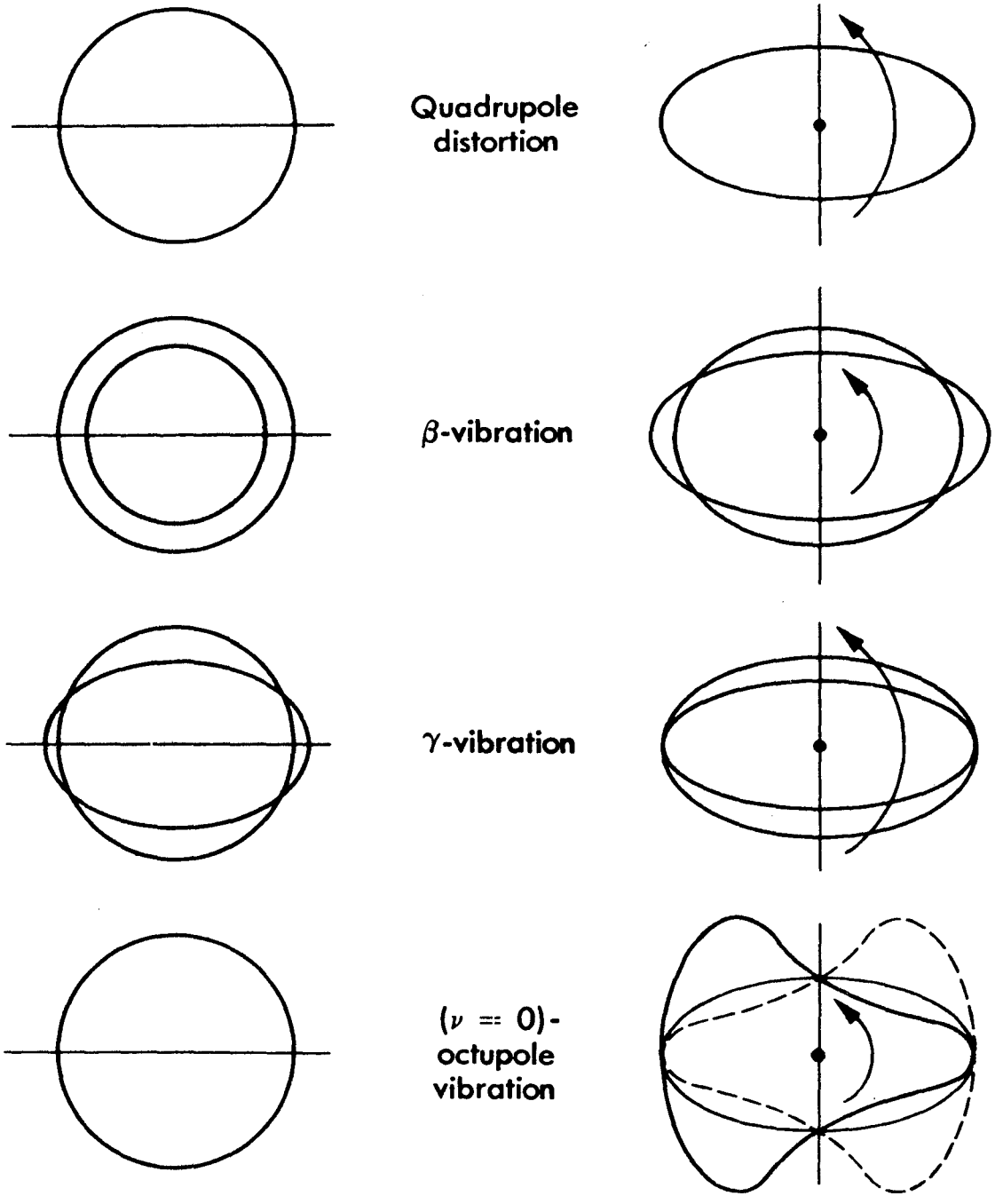

Figure A-1

An illustration of the simple vibrational modes of a deformed nucleus. (From reference 58).

Table A-1

B(E2) Excitation Values to Gamma and Beta Bands

Isotope	B(E2) Exc. $0^+ \rightarrow 2^+_{G.S.}$ e^2b^2	B(E2) Exc. $0^+ \rightarrow 2^+_\gamma$ e^2b^2	B(E2) Exc. $0^+ \rightarrow 2^+_\beta$ e^2b^2
^{152}Sm	3.40(12)[60]	0.068(12)[61] 0.085(15)[44]	0.061(14) 0.023(5)[44]
^{152}Gd	1.07(18)		
^{154}Gd	3.68(20)	0.13(5)	0.12(8)
^{166}Er	5.78(20)	0.21(4)	
^{232}U	9.9(1.2)	*	**

* Measured in ^{232}Th = 3 s.p.u. [50]
** Measured in ^{232}Th = 2 s.p.u.

value $\Delta K=0$ allows E0 transitions from the beta band, but the E0 transition does not compete with E2 except for large Z, Z greater than 80.

Transitions between the two vibrational bands are expected to be E2, since $\Delta K=2$. There is some disagreement on the predicted transition strength. Elliot[16] states that the strength should be intermediate between the collective and single particle value, while Bjornholm[59] remarks that the transitions should be retarded, as are two phonon transitions in spherical nuclei.

APPENDIX B

The fundamental paper describing the states of a particle in a deformed potential was written by Nilsson[54] in 1955. The single particle Hamiltonian (neglecting particle-particle and rotation - particle interactions) is

$$H = H_0 + C\,\vec{l}\cdot\vec{s} + Dl^2$$

$$H_0 = \frac{p^2}{2M} + \frac{M}{2}\left[\omega^2(x_1^2+x_2^2) + \omega_3^2 x_3^2\right]$$

With a change of variables, H_0 can be separated into two parts, H_{00} which is independent of angle, and H_β. The solutions can be found in several sets of base states. Nilsson used the representation $|N l \Lambda \Sigma\rangle$, corresponding to the following eigenvalues:

$$H_{00}\,|N l \Lambda \Sigma\rangle = \hbar\omega_0 (N+3/2)\,|N l \Lambda \Sigma\rangle$$
$$l^2\,|N l \Lambda \Sigma\rangle = l(l+1)\,|N l \Lambda \Sigma\rangle$$
$$l_3\,|N l \Lambda \Sigma\rangle = \Lambda\,|N l \Lambda \Sigma\rangle \quad |\Lambda| \le l$$
$$s_3\,|N l \Lambda \Sigma\rangle = \Sigma\,|N l \Lambda \Sigma\rangle \quad \Sigma = \pm 1/2$$

For axial symmetry, $j_3 = \Omega$ is a good quantum number, and solutions are

$$|N \Omega\rangle = \sum_{l\Lambda} a_{l\Lambda}\,|N l \Lambda \Sigma\rangle$$

Another basis has ℓ and s coupled, so that

$$H_{oo} |N \ell j \Omega\rangle = \hbar\omega_o (N+3/2) |N \ell j \Omega\rangle$$

etc.

The solutions are then written

$$|N\Omega\rangle = \sum_j c_{j\Omega} |N \ell j \Omega\rangle$$

Note that j is not a good quantum number, although $j_3 = \Omega$ is good. For large deformations, certain operator eigenvalues become constants of the motion. These are called asymptotic quantum numbers, and are usually given in the form

$$\Omega^\pi [N n_3 \Lambda]$$

This means that for a typical deformation the amplitude of any other state is small. The numbers $N n_3 \Lambda \Sigma$ are also used, since N determines the parity and $\Omega = \Lambda + \Sigma$. An example is $651\uparrow$ which is the same as $3/2^+ [651]$. The energy of these single particle states as a function of deformation has been given by Nilsson.

REFERENCES

1. C.Gunther and D. Parsignault, Phys. Rev. 153, 1297 (1967).

2. Y. Liu, O. B. Nielsen, P. Salling, and O. Skilbreid, Izv. Akad. Nauk, SSSR, Ser. Fiz. 31, 63 (1967).

3. L. Riedinger, N. Johnson, and J. H. Hamilton, Phys. Rev. Letters 19, 1243 (1967).

4. B. Mottelson, Tokyo Conf. on Nucl. Structure, p. 87 (1967).

5. S. Bjornholm, F. Boehm, A. B. Knutsen, and O. B. Nielsen, Nucl. Phys. 42, 469 (1963).

6. G. Alaga, Nucl. Phys. 4, 625 (1957).

7. P. De Brunner and W. Kundig, Helv. Phys. Acta 33, 395 (1960).

8. R. Stiening and M. Deutsch, Phys. Rev. 121, 1484 (1961).

9. J. H. Hamilton, A. U. Ramayya, L. C. Whitlock, and A. Muelenberg, Phys. Rev. Letters 19, 1484 (1967).

10. F. K. McGowan, R. O. Sayer, P. H. Stelson, R. L. Robinson, and W. T. Milner, Bull. Am. Phys. Soc., 13, 895 (1968).

11. R. Hager and E. Seltzer, Nuclear Data A4, 1(1968).

12. A. Bohr and B. Mottelson, Nuclear Structure, W. A. Benjamin (1968).

13. M. G. Mayer and J. H. O. Jensen, Theory of Nuclear Shell Structure, J. Wiley (1955).

14. N. Bohr and J. A. Wheeler, Phys. Rev. 56, 426 (1939).

15. A. Bohr, Dan. Mat. Fys. Medd. 26, #14 (1952).

16. J. P. Elliot, Collective Motion in Nuclei, Notes compiled by M. H. MacFarlane, Univ. of Rochester (1958).

17. E. Marshalek, Phys. Rev. 158, 993 (1967).

18. V. M. Michailov, Bull Acad Sci USSR, Phys Ser. 28, 225 (1964).

19. P. O. Lipas, Nucl. Phys. 39, 468 (1962).

20. Nuclear Equipment Corp. San Carlos, Calif. (May 1969).

21. G. T. Ewan and A. J. Tavendale, Can. J. Phys. 42, 2286 (1964).

22. R. L. Heath, Scintillation Spectrometry Catalog, IDO - 16880 - 1, AEC (1964).

23. J. M. Hollander, Nucl. Inst. and Meth. 43, 65 (1966).

24. F. S. Goulding, Nucl. Inst. and Meth. 43, 1 (1966).

25. R. L. Heath, Nucl. Instr. and Meth. 43, 209 (1966).

26. M. Mariscotti, Nucl. Instr. and Meth. 50, 309 (1967).

27. R. G. Helmer, R. L. Heath, M. Putnam and D. H. Lipson, Nucl. Instr. and Meth. 57, 46 (1967).

28. D. W. Marquardt, J. Soc. Indust. Appl. Math. 11, 431 (1963).

29. W. C. Davidon, ANL-5990 Rev. 1959 (IBM SHARE 3094).

30. L. Varnell, J. D. Bowman, and J. Trischuk, Nucl. Phys. A 127, 270 (1969).

31. L. Varnell and J. Trischuk, Bull. Am. Phys. Soc. 13, 1665 (1968).

32. E. N. Kaufmann, J. D. Bowman, and S. K. Bhattacherjee, Nucl. Phys. A119, 417 (1968).

33. J. B. Marion, Nucl. Data A4, 301 (1968).

34. C. M. Lederer, J. M. Hollander, and I. Perlman, Tables of Isotopes, 6th edition, John Wiley (1967).

35. R. A. Meyer, Phys. Rev. 170, 1089 (1968).

36. P. Alexander, and F. Boehm, Nucl. Phys. 46, 108 (1963).

37. W. F. Edwards, F. Boehm, J. Rogers and E. Seppi, Nucl. Phys. 63, 97 (1965).

38. J. M. Freeman and J. G. Jenkins, Nucl. Instr. & Meths. 43, 209 (1966).

39. E. Fairstein and J. Hahn, Nuclear Pulse Amplifiers, Tennelec Instr. Co. (1966).

40. J. D. Bowman, Thesis (unpublished) C.I.T. 1968.

41. E. Karlsson, E. Matthias, K. Siegbahn, Eds, Perturbed Angular Correlations, North Holland (1964).

42. B. Dzhelepov, N. Zhukovskii, and A. Maloyan, Sovt. Journal of Nucl. Phys. 3, 577 (1966).

43. B. Dzhelepov, N. Zhukovskii, and A. Maloyan, Sovt. Journal of Nucl. Phys. 1, 671 (1965).

44. E. Veje, B. Elbek, B. Herskind, and M. C. Olesen, Nucl. Phys. A109, 489 (1968).

45. C. J. Gallagher and V. G. Soloviev, Mat.-Fys. Skr. Dan. Vid. Selsk. 2, 1 (1962.

46. R. A. Meyer, Phys. Rev. 170, 1089 (1968), and J. G. Barredo, Bull. Amer. Phys. Soc. 14, p. 617 (1969).

47. J. Chwaszczewska, R. Kaczarowaski, J. Rudzinska, W. Kurcewicz and J. Zylic, Dubna Conf., p. 59, 1968.

48. V. M. Michailov, Izv. Akad. Nauk SSR (Ser. Fiz.) 30, 1334 (1966).

49. S. Bjornholm, J. Borgreen, D. Davies, N. Hansen, and J. Pedersen, Nucl. Phys. A118, 261 (1968).

50. E. Hyde, I. Perlman, G. Seaborg, The Nuclear Properties of the Heavy Elements, Vol. II, Prentice-Hall (1964).

51. D. R. Bes, P. Federman, E. Marqueda, and A. Zucker, Nucl. Phys. 65, 1 (1965).

52. I. M. Pavlichenkov, Nucl. Phys. 55, 225 (1964).

53. V. G. Soloviev and T. Siklos, Nucl. Phys. 59, 145 (1964).

54. S. G. Nilsson, Dan. Mat. Fys. Medd. 29, #16 (1955).

55. S. Bjornholm, J. Dubois, and B. Elbek, Nucl. Phys. A118, 241 (1968).

56. K. Kumar and M. Baranger, Phys. Rev. Letters, 17, 1146 (1966); Nucl. Phys. A110, 529 (1968).

57. K. Kumar, Nucl. Phys. A92, 653 (1967).

58. M. A. Preston, Physics of the Nucleus, Addison-Wesley (1962).

59. S. Bjornholm, Nuclear Excitations of the Heaviest Elements, Munksgaard (Copenhagen, 1965).

60. P. Stelson and L. Grodzins, Nucl. Data A1, 21 (1965).

61. Y. Yoshizawa, B. Elbek, B. Herskind, and M. Olesen, Nucl. Phys. 73, 273 (1965).